EUROPEAN ORGANIZATION FOR NUCLEAR RESEARCH

CERN-EP/81-69
10 July 1981

ELECTRON COOLING IN ICE AT CERN

Mary BELL, John CHANEY[1], Heiner HERR, Frank KRIENEN,

Poul MØLLER-PETERSEN, Guido PETRUCCI.

ABSTRACT

A general description is given of the CERN 'ICE' electron cooling experiment. The storage ring and the design and realisation of the cooling apparatus (electron gun and collector, the vacuum system, the magnetic system, the beam diagnostics, the high voltage stabilisation) are discussed. Some typical experimental cooling results are presented, and the cooling times are finally compared with some approximate theoretical estimations.

(Submitted to Nuclear Instruments and Methods)

---

1) Now at IRAM: Institut de Radio Astronomie Millimetrique, Grenoble.

1. INTRODUCTION

Electron cooling, a method of reducing phase space spread of an ion beam in a storage ring, was proposed by Budker[1] in 1966, and experimentally confirmed at Novosibirsk[2] in 1974-1975. Those tests were made with beams of relatively small emittances and momentum spread. The objective of the CERN Initial Cooling Experiment (ICE) was to cool a beam of larger phase space, such as would arise in the case of a secondary antiproton beam, in order to test the feasibility of a high luminosity proton-antiproton collider. The successful first experiments[3] were reported in September 1979. Here we

describe the work in more detail and report on the complete set of experiments.

Electron cooling is based on repeated interactions of ions (in this experiment protons), circulating in a storage ring, with a dense and 'cold' electron beam. The electrons have nearly the same mean velocity as the ions. They are introduced into a straight section of the storage ring and travel for a few metres together with the protons. Through Coulomb interaction the proton beam loses heat to the electron beam, which does not heat up appreciably because renewed continuously. After repeated passage through the cooler the protons tend to assume the same low temperature as the electrons.

The cooler and the storage ring are described in sections 2 and 3. Section 4 presents the experimental results, and some comparison with theory [4-10] is made in section 5.

2. ELECTRON GUN AND COLLECTOR

2.1 INTRODUCTION

Figure 1 is a photograph and figure 2 a diagram of the apparatus used for the production of the electron beam. This device is mainly composed of: a) a flat cathode electron gun which produces and accelerates the electrons; b) a drift space, in the central part of which electrons and protons travel together; c) a collector where the electrons are decelerated and finally absorbed. The gun and collector are inclined by 36 degrees (in the vertical plane) with respect to the horizontal central part of the drift region.

High vacuum is provided all along the electron and proton

trajectories. A nearly uniform longitudinal magnetic field is provided along the electron trajectories from the gun to the collector entrance. Inside the collector the magnetic field is strongly reduced and its lines diverge to the collector walls.

The nominal parameters of the apparatus are:

cathode voltage	-60kV
cathode diameter	5.08 cm
electron current	8.3 A(at full perveance, see below)
cocling length	3 m
magnetic field	≅ 700 gauss in the uniform region

The experiment showed that operation at high voltage was difficult due to excessive out-gassing which might be cured by a time-consuming process. For this reason in this experiment the gun was operated below the nominal voltage and current. The protons were of velocity .304c, or energy 46.63MeV. The corresponding electron energy is 25.40keV. To obtain axial electrons with this energy the cathode, because of space charge effects, had to be set a little lower than -25.40keV relative to the drift space, or last of the five anodes. The current drawn from the cathode, when space charge limited, is largely determined by the voltage of the first anode relative to the cathode. The voltages of the other anodes,and the axial magnetic field, are then chosen to minimise transverse electron motion (section 2.2). In this experiment the gun was usually operated in one of three space charge limited modes- 'full-perveance', 'half-perveance', and 'quarter-perveance'. In addition it was also possible

to run the gun in a temperature limited mode obtained from the half-perveance mode by reducing the cathode temperature. This mode is called in the following 'half-temperature'.

Hereafter we briefly describe the different parts of this device, its high voltage supply, the diagnostic methods used, and finally the performances obtained with different voltages and currents.

2.2 THE ELECTRON GUN

The gun (Figure 3) is mainly composed of a flat cathode of the dispenser type (various oxides in a tungsten matrix) surrounded by a Pierce shield and followed by five iris shaped anodes set on progressively increasing potentials. The cathode is 5.08 cm in diameter. It is heated by alternating current of 50 Hz up to about 1050 degrees centigrade. The central opening in all anodes is of 6 cm diameter.

The electron beam is, at the nominal working temperature, space-charge limited. The acceleration is of the resonant type [11] ; that is, the defocusing actions of the several anodes compensate one another. This compensation is possible because the whole system is immersed in a longitudinal uniform magnetic field, which forces the electrons with transverse momentum to spiral about the field lines. The problem is then to match the voltages of the various anodes to the spiralling of the electrons in such a way that the final transverse momentum is very small. Actually a small azimuthal drift must remain, because of the repulsive radial electric field set up by the space charge. This motion, inversely proportional to the magnetic field strength, can be regarded roughly as defining a

minimum transverse energy, or 'temperature'. For uniform current density the space charge electric field increases linearly with distance from the axis, and consequently the minimum temperature increases quadratically. In our case, for the nominal values, the azimuthal drift corresponds to a transverse energy of about 0.7 eV at the edge of the beam.

The gun was designed with the help of a computer program written by H. Herrmannsfeldt at SLAC [12]. Figure 4 is an example of computer output showing various electron trajectories in the gun. These trajectories wiggle in the accelerating region but become practically parallel to the axis after passage through the last anode.

Figure 5 shows the final transverse energy of various electrons calculated by the same program as a function of the magnetic field for a particular anode voltage setting (V_5 =60kV). Several minima appear in the graph showing values as low as 1eV at the edge of the beam, very close to the theoretical minimum. The sharpness of these minima indicates, on the other hand, how the transverse energy is critically dependent on the setting of the anode voltages and the magnetic field. We chose the minimum at 700 gauss which provides a sufficiently low temperature and eases the collector design (see section 2.3).

The computer program does not consider possible ionisation of the residual gas, nor the secondary electrons produced in the collector and travelling back into the acceleration region. These two effects may, in some cases, strongly alter the space charge and consequently the electron trajectories. They can even produce such an accumulation of ions as to increase considerably the vacuum pressure

[13]. The evaluation of the space charge effect has however shown that these two effects were practically negligible in our experiment.

2.3 ELECTRON COLLECTOR

The collector has the purpose of decelerating as well as possible the electron beam, or in other words of recuperating with the highest possible efficiency, the electron energy, and finally absorbing the electrons in such a way that secondary electrons emitted from its surface are unable to travel back toward the cooling region and the gun.

Figure 6 shows the collector structure. A cylindrical anode, cooled by water, absorbs the electrons. At the entrance an iris shaped magnetic shunt with an 84 mm central hole intercepts most of the magnetic field lines. This is followed by an electrode, also iris shaped, the 'repeller', set at a voltage only a few kV higher than the cathode and producing most of the decelerating field. Another electrode, the 'spike', is mounted on the collector axis and has the task of reflecting axial electrons towards the collector. Finally a third electrode, the 'mesh', of cylindrical shape , is coaxial with the collector and is intended mainly to repel some of the low energy secondaries.

The magnetic field in the collector is much weaker than in the drift region,and its liner of force diverge from the axis, tending to distribute the residual electron energy nearly uniformly over the collector surface. This magnetic field is shaped by five coaxial

coils powered by independent supplies. For minimum final electron energy the conservation of generalised angular momentum about the axis, (see also [13])

$$P_0 = m\gamma r^2(d\theta/dt) + erA_0,$$

where A_0 is the azimuthal component of the magnetic vector potential, and r is the radial position of the electron, leads for a given electron to the criterion

$$(r_0A_0)_{\text{drift tube}} = (rA_0)_{\text{impact on collector}}$$

i.e. an electron moving on a magnetic field line in the drift tube should meet the same field line at the point of impact on the collector. In the drift tube $m\gamma r^2(d\theta/dt) \simeq 0$, whereas the same term on the collector surface represents non-recuperable energy. This term is about zero if the above criterion is satisfied. Most of the magnetic field lines along which the electrons move, can be made to re-enter the magnetic shunt, before they coincide with the point of impact on the collector surface. Hence low energy secondary electrons gyrate around a field line which emerges from the shunt and these electrons are then captured by the repeller. A computer program has been developed to determine suitable parameters which most nearly satisfy the above criterion [14]. Figure 7 shows some computed trajectories. The magnetic field shape on the axis is also shown.

2.4 VACUUM SYSTEM

High temperature surfaces, many geometrical constrictions due to the complex shapes, high electric field, and clean optics, all produce the need for a good vacuum. All the materials composing the system

have been selected for this purpose, carefully cleaned, and each part baked out at the highest possible temperature for many hours. The dispenser cathode is a strong source of gas, some of it trapped in the body and escaping only slowly, and some created during the cathode formation (carbonates transforming into oxides CO, CO_2,etc.). Furthermore, in spite of the baking out, all the collector surfaces and the various anodes, submitted to electron bombardment, outgas strongly. For all these reasons acceptable vacuum conditions are obtained only after many weeks of running with increasing voltages and currents. In fact during the first weeks the operation had to be stopped frequently to avoid instabilities and breakdowns.

The necessary pumping speed was provided by three sputter ion pumps of 220 lt/sec, the pre-vacuum being established by a turbo_ molecular pump of 250lt/sec. Two titanium sublimation pumps were also installed in the system and allowed further improvement of the vacuum. These last pumps have been useful, particularly in the final stage of our tests when the best vacuum conditions were reached ($\simeq 2.10^{-10}$Torr with cold cathode and zero current, and $\simeq 4.10^{-10}$Torr when operating the system at ≃30kV and 3A). The main elements of the vacuum system can be seen in Figure 2.

2.5 THE MAGNETIC SYSTEM

The magnetic field has the purpose of guiding and restricting the transverse motion of the electron beam. We require a good homogeneity (around 10^{-4} in $\delta B/B$) of this field to avoid an increase of electron temperature and ,in the cooling region, reduced efficiency due to bad velocity matching. The main longitudinal, uniform, magnetic field

following the electron trajectories up to the collector entrance is produced by three solenoids, located along the gun region, the cooling region, and the region preceding the collector, and two toroids located in correspondence with the 36 degree bends. The field of the toroids is matched to the field of the adjacent solenoids at the beam axis. Two small dipole magnets ,perpendicular to the bending plane, are mounted inside the toroids and deflect the electrons by the 36 degree angles. In this way one can avoid the increase of transverse energy($\simeq$2eV) which would be produced for bends induced by the toroidal fields alone.

The solenoidal and toroidal windings are made by two layers of 15x15mm^2 copper conductor. These windings are mounted inside iron cylinders and sector-shaped cases,1.5cm thick,providing the return path of the magnetic flux. The iron plates mounted at the ends of each element contain the windows needed for the passage of the electron and proton beams,the pump ducts and the various diagnostic and control apparatus. All the main windings of the system are connected in series and powered by a single supply, but variable shunts,mounted across the windings, allow a relative adjustment of the field strength.

Correcting coils have been mounted to compensate for a missing turn in the centre of the split solenoid of the cooler section. Furthermore, dipole coils, powered separately, producing both horizontal and vertical fields have been mounted on each section of the system, providing the possibility of tilting the main field by a few mrad. A careful field mapping has allowed the determination of the various corrections needed. The five coils shaping a

progressively decreasing field inside the collector,(50gauss - 1gauss, see also Figure 7), were adjusted individually during operation in order to maximize the power recuperation of the device.

The deflection of the proton beam in the horizontal plane due to the toroidal magnetic field was compensated by a correction magnet at each end of the system((6) on Fig.2).

2.6 THE DIAGNOSTICS

The most usual tuning procedure was based on a continuous checking and recording of the voltages on and currents absorbed by the various electrodes,both on the gun and on the collector side. The basic assumption here was that a centred well-cooled beam corresponded to conditions of minimum loss and high energy recuperation. These optimum conditions correspond also to the lowest possible pressure in the system for given cathode voltages and electron currents. A fast rising pressure was usually interpreted as a sign of wrong optics.

During the first weeks of operation,four pairs of 20micron tungsten cross-wires were mounted along the electron trajectories at positions visible to TV cameras. These wires glowed at the parts hit by electrons, thus providing clear information about the beam size and position. This method, which has only a small disturbing effect on the beam optics, is unfortunately feasible only up to a certain electron energy and density, above which the temperature of the wires increases too much and the wires are quickly destroyed due to recristalisation brittleness. This method might of course be extended to higher energies by pulsed operation.

The evaluation of the transverse electron temperature, that is, their transverse energy, is particularly difficult. The main evidence, independent of the cooling process itself, comes from the rate of formation of neutral atoms in the cooled beam[2]. This is sensitive to the velocities of electrons relative to protons. The neutral atoms form a beam detected at the neutral beam monitor, (11) on Fig.8. The results are tabulated as 'transv temp' in TABLE 1. They are the average temperatures of the electron beam over the cross-section of the cooled beam(almost the central area of the electron beam). The edge of the beam is expected to be 'hotter' from the computer calculation mentioned above.

Another measurement of temperature was attempted by a method suggested by C.Rubbia[15] and developed by B.Schnizer and E. Farnleitner[16],C.Taylor and S.Hancock[17]. This method is based on the detection of the synchrotron radiation emitted by the electrons spiralling in the magnetic field. This radiation, in the cm range, travels along the vacuum chamber as in a wave guide and is picked up by an antenna[17]. As an example,we show in Fig.9 an energy spectrum measured for electrons of 25.9kV and a field of 454.3 gauss. This spectrum extends from about .85GHz to about 1.65GHz as expected but has a large dip in the centre. The radiated power is calculated to be, in our case, of the order of 4.10^{-11} watt for the P/2 gun(1.2A at 25kV) supposing an average transverse electron energy of 1eV. In spite of the difficulty in reaching an absolute temperature estimate, due to the presence of severe noise, this method has aided us in making a fine adjustment of the gun parameters.

2.7 HIGH VOLTAGE STABILISATION AND CONTROL SYSTEM

A schematic diagram showing the principle of operation of the high voltage system is given in Fig.10. In this system beam power is recuperated in the collector so that the high voltage power supply has only to provide power corresponding to beam losses and inefficiency.

High voltage in the range 0-100kV, 0-200mA was generated with a conventional 3-phase transformer supply which was rectified and smoothed to give a ripple of about 1%. The DC stability of the rectified supply was held to better than 2% with three 220V mains stabilizers at the transformer inputs. Further stabilization was achieved with a transistor bank connected between ground and the HV supply. An error signal produced by comparing the signals from a HV divider and a reference voltage source was used to drive the transistor bank. In this way, a DC stability of 10^{-5} and ripple 10^{-4} (rms) was obtained. The total dynamic range of the transistor bank was approximately 1kV. The ripple had a fundamental frequency component of 300 Hz. A compromise between high DC stability and low ripple had to be made since they were dependent on the control loop gain and amplification response time. This low ripple had negligible consequences on the cooling forces.

Modulation of the high voltage, which was used as a diagnostic means for studying electron cooling,was made possible by adding low amplitude signals to the reference voltage. Care was taken to ensure that these signals were free from noise, such that DC stability was maintained even during modulation. The amplitude of the high voltage modulation could be varied between 0 and 300V with a minimum time

constant of about 2ms. The high voltage could be made to follow any type of waveform from a pulse/waveform generator.

Control and monitoring of all devices at high voltage was made with fiber-optic links. In the case of control, conventional fiber optic/relay switches were used to operate power supplies and equipment inside the Faraday cage. The monitoring of currents and voltages was made by means of a single multiplexed frequency modulated fiber-optic link. In this system signals were first detected with isolation amplifiers (up to 3kV isolation), their outputs fed into a FET analog multiplexer and converted into a frequency between 0 and 10kHz. This frequency was then transmitted by a fiber optic cable to the control room where conversion back into voltage was made. Measuring resolution was better than 0.1%. A total of 8 channels were used for monitoring.

2.8 OPERATION OF THE ELECTRON COOLING DEVICE

One of the most critical points for assuring good performance of such a high power electron beam device is the recuperation of beam power. Power losses are due to current losses and to the fact that the collector voltage has to be higher than the cathode voltage.

The efficiency in current collection, η_c, power recuperation, η_p, as well as the voltage efficiency η_v, are defined as

$$\eta_c = 1-\delta I/I \qquad \eta_p = 1-\delta P/P \qquad \eta_v = 1-V_{co}/V_s$$

In these equations δI and I are the loss and total beam current respectively; whereas V_{co} is the positive collector voltage measured with respect to the cathode.

The power loss δP on the total beam power $P=V_5 I$ consists of two terms

$$\delta P = V_5\, \delta I + V_{co}\, I$$

of which the first term is supplied by the high voltage supply and the second by the collector supply.The energy is dissipated as heat on the grounded vacuum chambers ($v_5\ \delta I$) and in the collector ($V_{co}\ I$) and will cause both outgassing and desorption of residual gas molecules. The task is hence to minimize both δI and V_{co} to obtain the best performance of the device.

There are several factors which affect δI of which we mention:

1) Residual gas scattering, which however at pressures $<10^{-8}$ Torr and at sufficiently high energy is not significant.

2) Imperfections in guiding and collector fields.

3) Secondary electrons emitted from the collector surface and escaping from the collector aperture.

4) Lack of matching of magnetic potentials may lead to backstreaming electrons.Depending on the accuracy in the matching of the magnetic potentials the minimum collector voltage V_{co} is also determined (see 2.3).

We now discuss more fully the above points 2),3), and 4).

Guiding Field Imperfections.

Variation of the solenoidal field for fixed gun high voltage showed an oscillatory dependence of $\delta I/I$ with a peak to peak

variation of around 10^{-3}. The frequency of these oscillations corresponded to 2π phase advance of the cyclotron motion over the full length from gun to collector aperture. This indicates that, because the effective collector aperture is just barely big enough (see fig 7), the electron beam has kept its coherent ripples all the way to the collector. The variation of the beam diameter, found in this way, is of the order of magnitude of that expected from computer calculations for the gun using the SLAC-program(≃.1mm).

Secondary Emission.

The secondary electrons in the energy spectrum which may limit the collection efficiency are mostly elastically scattered, whereas the slow 'true' secondaries are energetically trapped and to a first approximation guided towards the repeller by the magnetic lines of force. The elastically scattered electrons may energetically escape from the collector and cause a loss of efficiency of the device.

By increasing the negative voltage of the mesh and so creating a retarding field along the collector surface the loss current was progressively reduced. As the extension of an equipotential line of the retarding field is determined by the voltage of the mesh this increase causes suppression of secondary electrons further towards the end of the collector. For the best mesh voltage found, which also corresponded to the maximum allowed due to insulator and field emission problems the voltage of the mesh was even below that of the cathode($V_{co} - V_{me}$ up to 2kV).

Minimum Collector Voltage

Decreasing the collector voltage below a certain value caused a

dramatic increase in loss current and the beam became very unstable. This minimum collector potential is mainly determined by the degree of success in recuperation of rotational energy of the gyrating electrons, but may also be limited by space charge instabilities.

Fig.11 shows the collector perveance defined as $P_{co} = I.V_{co}^{-3/2}$ as a function of beam current I for the electron gun operated in full- and half-perveance modes. The magnetic fields have been scaled according to the square-root of the high voltages(roughly). One observes that the collector perveance reaches a saturation value of approximately

$$4.10^{-5}\ \mathrm{AmpVolt}^{-3/2}$$

The maximum efficiency of power recuperation is then

$$1 - V_{co}/V_5$$

which for the half and full perveance gun gives $\eta_p = .96$ and .94, respectively.

On Fig.12 we have plotted the relative loss current as a function of electron gun high voltage for the half- and full-perveance gun. The solenoidal magnetic field has to be scaled with the square root of the gun high voltage (in nonrelativistic approximation). The collection efficiency is nearly independent of total beam current but becomes continuously worse at higher voltages. This indicates in general some imperfections in the beam optics and in particular at the collector aperture. The minimum relative loss current obtained with the device is $\delta I/I = 7.10^{-4}$,but this was obtained running the

gun alone after the experiment reported here.

Experiments are at present being continued to change the beam optics at the deceleration into the collector.

TABLE 1 summarizes the parameters obtained with the electron gun. Note that voltages in the table are relative to the cathode, except that mesh and repeller voltages are relative to the collector. In fact it is the drift space, and fifth anode, which are earthed. The voltages and currents of the table are representative values; the actual values varied a little from day to day with the proton energy. Also given in TABLE 1 are various derived quantities entering into theoretical calculations. The transverse temperatures have been estimated from the neutral rates using a formula given in reference[18].

TABLE 1

		full P	P/2	P/4	T/2	unit
beam current	I	2.234	1.278	.660	.599	Amps
anode volts	V_5	26.23	25.90	25.60	25.6	kV
	V_4	.853	.793	.748	.793	V_5
	V_3	.825	.643	.553	.643	V_5
	V_2	.620	.446	.356	.446	V_5
	V_1	.519	.329	.204	.329	V_5
anode currents	I_1	.120	.120	.560	.360	mA
	I_2	-.400	-.120	-0	-.120	mA
	I_3	0	-.600	-.120	-.480	mA

	I_4	-2.1	-1.0	-.600	-1.2	mA
current loss	$\delta I/I$	2	2	2	5	10^{-2}
power loss	$\delta P/P$	8.0	7.6	5.8	9.3	10^{-2}
collector pot	V_{co}	1.60	1.20	1.00	1.2	kV
mesh volts+	V_{me}	-600	-600	-600	-600	V
repeller volts+	V_{re}	-200	-200	-200	-200	V
magnetic field	B	461	519	416	516	G
mag stability	$\delta B/B$	5	5	5	5	10^{-5}
HV stability	$\delta V_5/V_5$	6	6	6	6	10^{-5}
pressures	PG	10	3	2	3	10^{-10}Torr
	PC	10	3	2	3	10^{-10}Torr
eff length	L	3.0	3.0	3.0	3.0	m
axial vel	V_o	.3040	.3040	.3040	.3040	c
current dens	J_e	1102	631	326	296	Am^{-2}
beam diameter	2a	5.08	5.08	5.08	5.08	cm
outer diameter	2b	9.8	9.8	9.8	9.8	cm
electron dens	n_e	.755	.432	.223	.202	10^{14} m^{-3}
neutral rate	R_0	750	310	140	65	sec^{-1}
(per 10^8protons)						
transv temp	T_t	.15	.24	.30	.85	eV
transv vel	V_t	2.52	3.19	3.56	6.00	10^{-3} V_o
screening rad	ρ_{max}	.0469	.0784	.122	.216	cm
collision rad	ρ_{min}	.480	.300	.241	.0847	10^{-6} cm
Larmor rad	r_l	2.83	3.19	4.43	6.025	10^{-3} cm
adiab.scr.rad	ρ_{amax}	.0651	.0861	.120	.126	cm
(at V_{it} =3.5 10^{-3} V_o)						
	(2.)	.0372	.0492	.0684	.0718	cm
	(1.5)	.0279	.0369	.0513	.0539	cm

Coulomb log	L_c	11.49	12.48	13.13	14.75
fast Coul.log	L_f	8.68	9.27	9.82	11.17
adiab. Coul.log	L_a	3.13	3.30	3.30	3.04
(at V_{it} =3.5 10^{-3} V_o)					
	(2.)	2.58	2.74	2.74	2.48
	(1.5)	2.29	2.45	2.45	2.19

+relative to collector

Considering that the design has been to a large extent based on computer calculations and that no modifications of the initial assembly has been performed, the performance of the device has been very satisfactory.

3. THE ICE STORAGE RING

The ICE storage ring (Fig.8) is a strong focusing, combined function machine for protons. It has four magnetic sectors and four straight sections. The magnetic sectors consist of ten alternating gradient magnets. Pole face windings, mounted on the D-magnets, allow the tune of the machine to be changed. As the experiments were carried out at a proton energy of 46MeV, which is close to the transition energy of the ring, the tuning range was sufficient to operate the machine above and below the transition energy. The protons were obtained by extracting from the PS(S.S.74), after a special deceleration cycle, a single or a double bunch of protons of the wanted energy. These protons were transferred to the ICE area (about 140m away) and injected into the ring by means of a pulsed inflector and a full aperture kicker. By injecting one proton bunch

into the ICE ring, about 2.10^8 particles could be stored.At an average vacuum pressure around the ring of 2.10^{-9} Torr, the beam lifetime was about 2 min. without cooling.

Several diagnostic devices have been used to study the cooling process:

1) A horizontal and vertical set of wire-chambers allowed the measurement of the production rate and the transverse position of hydrogen atoms formed by recombination of e- and p in the cooling sections. The H^0 -atoms leave the storage ring at the end of the cooling section by a hole in the following magnetic sector. They are stripped in a foil and then detected by the wire chambers. The wire chambers' readings are recorded and processed by a microcomputer (CAVIAR)[19]. The wire-pitch of the chamber was 1mm.

2) A set of horizontal and vertical scrapers allowed a destructive measurement of beam size and position.

3) A horizontal and a vertical beam profile monitor [20],developed by G.Stefanini, allowed the non-destructive observation of the transverse beam size and the beam position. The operation of this monitor is based on ionisation of the rest gas by the circulating protons. Electrons created in this way are electrostatically accelerated perpendicular to the beam direction. They are guided by a magnetic field, parallel to the electric field, towards a phosphor screen where they create an image, the intensity distribution of which is proportional to that of the corresponding circulating protons. The image is scanned by a slit mounted on a rotating drum and the light traversing the slit is collected by a photomultiplier. The resolution of this device, depending on many factors, was of the order of 2.5mm FWHM in both planes.

The minimum possible scanning time, under the conditions of the experiment, was 200 msec, short enough to follow the cooling process in detail.

The signals of the beam profile monitor were processed by a CAVIAR system, and displayed on a TV-screen.

4) A set of longitudinal Schottky noise pick-ups[21] allowed the measurement of the momentum spread. Using a commercial frequency analyser the momentum spread could be measured every 200 to 2000 ms depending on the required resolution.

Applying noise in a small band around the third harmonic of the revolution frequency on a longitudinal wide-band kicker it was also possible to influence the momentum-spread and to set it to a fixed value. This technique allows momentum cooling experiments with well defined starting conditions.

For the cooling studies the beam could be excited in the transverse direction in a coherent way by the full aperture kicker(FAK).

Furthermore the ICE-ring is equipped with a special RF-cavity which allows the beam to be bunched on the first harmonic of the revolution frequency. This allowed studies of bunched beam cooling. It also gave the possibility of beam-stacking by injecting new protons into the ring at the moment when the stack was circulating in the ring region opposite to that of injection. The newly injected particles were then cooled into the bucket. With this technique, experiments could be carried out also at higher intensities($\simeq 2.10^9$ circulating protons).

The main parameters of the ICE ring are indicated in TABLE 2.

TABLE 2 (ICE ring data)

maximum[+] and minimum momentum	2.1 and 0.30 GeV/c
circumference	74.38m
number of focusing periods	4
aperture of vacuum chamber	$a_h = \pm 76$mm
(minimum values)	$a_v = \pm 28$mm
working point	$Q_h = 1.71^{++}$
	$Q_v = 1.16^{++}$
(value of transition γ)	$\gamma_t = 1.3063$
acceptances	$E_h = 80\pi$ mm.mrad
	$E_v = 40\pi$ mm.mrad
	$\Delta p/p \simeq \pm 0.31\%$
cooler length/orbit length	4.10^{-2}

[+] The maximum momentum was used for stochastic cooling experiments.

[++] These values correspond to a working point below transition and were commonly used during this experiment.

4. EXPERIMENTAL RESULTS

4.1 THE COOLED BEAM

Except where otherwise stated we will report results with a few times 10^8 protons in the ring, and with the gun operated in P/2 mode, and an average vacuum pressure of 2.10^{-9} Torr.

With the electron and proton beams well matched in velocity (to about 4 parts in 10000) and direction (to about 5.10^{-4} radian) cooling was immediately observed[3]. Within a time of the order of one second the proton beam stabilized with greatly reduced spreads in angle and energy.

A mean life of about 140 minutes was observed for the cooled beam, as compared with about 2 minutes for the uncooled beam mentioned above. The first lifetime corresponds to the calculated value for losses produced by single scattering on the rest gas.

To measure the cooled beam diameters or angular divergences, we have employed, as described before, three methods:

1) neutral beam profile

2) scraper tests

3) horizontal beam profile monitor

1) Figure 13 shows an example of the cross-section of the neutral atom production as seen by the 2-dimensional MWPC, integrated over successive time intervals of 5 sec. during the cooling process. The rms horizontal and vertical widths are 2.6mm and 2.5mm respectively. The corresponding angular divergences are

$$\theta_h(\text{rms}) = 2.3\ 10^{-4} \qquad \theta_v(\text{rms}) = 2.3\ 10^{-4}$$

2) The effect of horizontal and vertical scraping on beam intensity allowed measurement of beam sizes at the scraper positions (9 and 10 in Fig.8). The full-width-half-maximum beam sizes so found were

$$a_h(Q2) \simeq 2.3\text{mm} \qquad a_v(Q2) \simeq 2.8\text{mm}$$

From the lattice parameters the corresponding angular divergences in the cooling region are

$$\theta_h(\text{FWHM}) \simeq 2.4\ 10^{-4} \qquad \theta_v(\text{FWHM}) \simeq 2.3\ 10^{-4}$$

consistent with the above results from the neutral beam profile, which yield a beam size in the cooler region below 1mm FWHM. The distribution has a central gaussian part and tails.

3) Figure 14 shows profiles observed by the horizontal BPM with different slit widths in the drum of the mechanical scanning system, and for a circulating proton intensity of approximately 2.10^8 particles. For (a) the slit width is 1mm, and the apparent beam FWHM is 4.5mm. For (b) the slit width is .3mm, and the apparent beam FWHM is 2.4mm. The demagnification factor is in both cases 1:3, and so the intrinsic resolution FWHM of the device is 3mm and 1mm in cases (a) and (b), respectively. The determination of profile width was thus limited by the resolution of the device, and only an upper limit of 2.4mm(FWHM) could be established.

For measurement of equilibrium momentum spread the longitudinal pickup sensitive to Schottky noise was used. Figure 15a shows an example of two Fourier analyses of Schottky noise,taken at the beginning and end of the cooling process, at the 24^{th} harmonic of the revolution frequency. Horizontally is plotted frequency, small variation of which is proportional to small variation of momentum. The signal strength, plotted vertically, is proportional to the square root of the particle density. Fig.15b shows the Schottky noise of a cooled beam of 8.10^6 protons. Its momentum spread is

$$\delta p/p = 4.10^{-5} \qquad \text{(FWHM)}$$

We found, as did the NAP-M group, that momentum spread is dependent on proton intensity, mainly due to intra-beam scattering. Results with various proton intensities are shown in Figure 16 , for the T/2 and P/2 guns. Moreover it is known that for very cool very intense ion beams the interpretation of the Schottky signal is not quite trivial[22]. Applying a suitable correction to the experimental number

we finally find for 10^8 protons and the P/2 gun

$$\delta p/p \simeq 6.10^{-5} \quad \text{(FWHM)}$$

4.2 BETATRON OSCILLATON COOLING

Horizontal betatron oscillations were excited artificially on the cooled beam by a short (700nsec) coherent pulse from the Full Aperture Kicker. Damping was then followed on the horizontal beam profile monitor. Repeated excitation to various amplitudes were made and the total damping time measured as a function of excitation amplitude. Figure 17 shows an example of such observations. The time between frames is 800 msec. The total damping time, down to the resolution of the monitor, is here about 7sec . The damping could also be observed with the neutral atom profile.

The horizontal acceptance of the storage ring, taking into account closed orbit distortion, limited the excitation amplitude to about 3.8mrad. The minimum observable amplitude was determined by the resolution of the horizontal beam profile monitor.

Figure 18 shows results for various gun modes. The total damping time down to the BPM resolution is shown as a function of initial excitation amplitude. The slopes of these logarithmic plots define cooling times

$$t = \theta_t/(d\theta_t/dt)$$

where θ_t is the amplitude of betatron oscillation. The resulting cooling times are tabulated in TABLE 3 as t(exp). In the fourth case, T/2, where some dependence of slope on amplitude shows up

clearly, it is the value at 2mrad which is tabulated.

To examine the dependence of betatron oscillation cooling on longitudinal electron velocity spread, such a spread was excited by 1kHz sine wave to the gun high voltage. Figure 19 shows , for the P/2 gun, the decrease of damping rate (solid triangles) with increasing longitudinal electron velocity spread, as observed already by the NAP-M group. Also given in this figure is the longitudinal proton momentum spread of the cooled beam (solid circles) measured by the longitudinal pickup.

4.3 MOMENTUM COOLING

The momentum cooling force, for small betatron amplitudes, was measured separately by first cooling the beam and then suddenly increasing the gun voltage and observing the subsequent acceleration of protons. By voltage increases in the range 2V-300V fractional relative velocities in the range 5.10^{-5} to 6.10^{-3} were created. The proton acceleration was observed as a change of revolution frequency, with the longitudinal pickup, and as a change in radial beam position, with the horizontal beam profile monitor. The drag force is then

$$F_1 = (p/\eta)\ (df/dt)/f$$

where η is the storage ring parameter

$$\eta = (p/f)(df/dp)$$

in terms of rate of frequency change, and

$$F_1 = (p/\alpha_p)\ (dr/dt)$$

where α_p is the storage ring momentum compaction function

$$\alpha_p = p\ (dr/dp)$$

in terms of rate of radius change. To be independent of computer calculations the machine parameters η and α_p were measured, by observing equilibrium frequency and radial position as functions of gun voltage for small variations of the latter.

Figure 20 shows results on F_1 as a function of relative velocity

$$\theta_1 = (V_0 - V_{i1})/(V_0)$$

where V_0 is the axial electron beam velocity. Note that this formula is only approximate, since the space charge induced velocity gradient ought to be taken into account. The open circles are for the P/2 gun, and the inverted triangles also but with a 1kHz sine wave of 50V peak-to-peak amplitude superimposed on the step voltage. The increase in steepness of this second measurement for lower relative velocity indicates that we undid some of the 'flattening' (see section 5), and moved nearer the symmetrical electron velocity distribution. The points in Figure 20 are T/2 measurements.

5. COMPARISON WITH THEORY.

Various authors have given formulae for the cooling or 'drag' force [4-10]. We will just quote results here. In the absence of magnetic field the force is

$$\vec{F} = K\int d^3\vec{V}_e \, f(\vec{V}_e) \, (\vec{V}_e - \vec{V}_i) c^2 / |\vec{V}_e - \vec{V}_i|^3 \qquad (5.1)$$

where

$$K = (4\pi n_e r_e^3)(m_e c^2 / r_e) L_c \qquad (5.2)$$

n_e = electron density

$r_e = 2.818\ 10^{-15}$ m

m_e = electron mass

$c = 3.\ 10^8$ m/sec

$\vec{V}_i$ = proton velocity

$\vec{V}_e$ = electron velocity

and $f(\vec{V}_e)$ is a normalised electron velocity distribution:

$$\int d^3\vec{V}_e \, f(\vec{V}_e) = 1 \qquad (5.3)$$

The 'Coulomb logarithm' L_c we take as

$$L_c = \ln(\rho_{max} / \rho_{min}) \qquad (5.4)$$

with

$$\rho_{min} = r_e (c/W)^2 \qquad (5.5)$$

$$\rho_{max} = r_e (W/c) / \sqrt{(4\pi n_e r_e^3)}, \qquad (5.6)$$

where W is a typical proton-electron relative velocity.

These formulae are most properly interpreted as apolying in a

frame of reference moving with the electrons. This has been attended to in the computer simulation [23]. But in the present qualitative discussion, neglecting relativistic corrections, we take the formulae to hold in the lab.frame.

For what follows it is convenient to define also:

V_o = mean electron velocity on axis

$$\vec{U}_i = \vec{V}_i - \vec{V}_o \qquad (5.7)$$

= proton velocity relative to electron beam

V_t = root mean square transverse electron velocity

V_l = root mean square spread of longitudinal electron velocity

Let us first imagine the distribution to be 'Maxwellian',

$$f(\vec{V}_e) = (m_e/(2\pi T_t))\exp(-m_e V_{et}^2/(2T_t)) \sqrt{(m_e/(2\pi T_l))}\exp(-m_e (V_{el}-V_o)^2/(2T_l)) \qquad (5.8)$$

corresponding to

$$V_t = \sqrt{(2T_t/m_e)} \qquad (5.9)$$

$$V_l = \sqrt{(T_l/m_e)} \qquad (5.10)$$

For equal temperatures

$$T_t = T_l = T \qquad (5.11)$$

and small proton relative velocities U_p

$$|\vec{U}_i| = |\vec{V}_i - \vec{V}_o| \ll V_t \qquad (5.12)$$

and treating K as constant, one finds

$$\vec{F} = (4/(3\sqrt{\pi}))\, K\, ((\vec{V}_o - \vec{V}_i)/c)(m_e c^2/(2T))^{3/2} \qquad (5.13)$$

corresponding (in the absence of any other forces) to exponential cooling with

$$U_i \text{ varying as } \exp(-t/t_o)$$

where

$$t_o = (3/(16\sqrt{\pi}))(m_p/m_e)(2T/(m_e c^2))^{3/2}/(n_e r_e^2\, c L_c) \qquad (5.14)$$

Note that for damping of energy (or temperature) the exponential cooling time is halved, for

$$(\exp(-t/t_o))^2 = \exp(-2t/t_o) \qquad (5.15)$$

Note that $t_o/2$ is the often quoted cooling time of Spitzer[24] with

$$T_i/m_i \ll T_e/m_e$$

This has served well in preliminary discussion of the ICE experiment [25]. Multiplication of t_o by the duty cycle factor

$$(\text{machine circumference/cooler length}) = 1/d = 25$$

gives the 'nominal cooling time' (t_{nom}) of Table 3. We have taken $W = V_t$ in (5.5),(5.6).

More realistic than the symmetric Maxwell distribution, with $T_l = T_t$, is the 'flattened' distribution [5,6] with

$T_l = 0.$

Then instead of (5.13) we now have

$$F_t = -(V_{it}/c)\sqrt{\pi}\, K\, ((m_e c^2)/(2T_t))^{3/2} \qquad (5.16)$$

$$F_l = \pm K\, 2(m_e c^2/(2T_t)) \qquad (5.17)$$

where the undetermined sign is opposite to that of U_l. The transverse force is about twice as big as before. The longitudinal force is much increased. In particular, it does not go to zero with U, so that for small U longitudinal damping is much faster than transverse. Actually for very small U the approximations fail, (for example the constancy of the logarithm) and F_l again approaches zero, (Sørensen[9]), but we will not consider this here.

It remains to consider magnetic effects. The cooling collisions are conventionally divided into 'fast' and 'adiabatic'. The fast term is just (5.1) but with the Coulomb logarithm replaced by

$$L_f = \ln(r_l/\rho_{min}) \qquad (5.18)$$

where r_l is a typical Larmor radius.

$$r_l = m_e V_t/(eB) \qquad (5.19)$$

The 'adiabatic term' is rather complicated in general, and we will consider here only special cases, of pure transverse and pure longitudinal motion.

$V_{it} = 0.$

In this case (no betatron oscillation) the adiabatic contribution vanishes. We are left with (5.17) with L_c replaced by L_f(5.18). This

gives for the various gun modes the values listed in TABLE 3, which includes also the maximal experimental values. An example of P/2 and T/2 gun measurements can be seen in Fig.20, (to be multiplied by a factor 1/d = 25 to obtain the force in the cooler as distinct from the average round the orbit). Given the roughness of the theory used here the discrepancy between theory and experiment (a factor of about 2) is not surprising.

$V_{i1} = 0$

In this case, of pure betatron oscillation, the adiabatic contribution to the drag force is

$$(K/2)(L_a/L_c)(-V_{it}\,c^2)/|V_{it}|^3 \qquad (5.20)$$

with

$$L_a = \log(\rho_{amax}/r_1) \qquad (5.21)$$

and $$\rho_{amax} = (V_{it}/c)\,r_e/\sqrt{(4\pi n_e\, r_e^3)} \qquad (5.22)$$

The instantaneous (V_{it} dependent) cooling rate is then

$$-(dV_{it}/dt)/V_{it} = A + B/|V_{it}|^3 \qquad (5.23)$$

with

$$A = (L_f/L_c)(3\pi/4)/t_{nom} \qquad (5.24)$$

$$B = (L_a/L_c)(3\sqrt{\pi})/8)V_t^3/t_{nom} \qquad (5.25)$$

We have still to allow for the fact that V_{it} is not constant in the absence of cooling, but oscillating. Let V_{itmax} denote the maximum value in the course of a betatron oscillation, now taken to be purely

vertical or purely horizontal. Then averaging over the oscillation we find the cooling rate $(1/t)$ for the amplitude of oscillation

$$(1/t) = -(dV_{itmax}/dt)/V_{itmax} = (1/t_f) + (1/t_a) \qquad (5.26)$$

with

$$t_f = t_{nom}\,(L_c/L_f)(8/(3\pi)) \qquad (5.27)$$

$$t_a = t_{nom}\,(L_c/L_a)(8/(3\sqrt{\pi}))(V_{itmax}/V_t)^3/R \qquad (5.28)$$

where

$$R = (2/\pi)\ln(2V_{itmax}/V_{itmin}) \qquad (5.29)$$

In this expression V_{itmin} is a lower cut-off at which the treatment for some reason fails[26]. For example, the longitudinal electron velocity spread V_l might no longer be negligible, or the logarithm L_a might no longer be sufficiently constant. More important in our case, probably, is that horizontal and vertical betatron oscillations are strongly coupled by the cooler magnetic field, so that when one component of V_{it} is small the other need not be. Without attempting here to analyse this in detail, let us see what happens if we quite arbitrarily take

$$R = 1 \qquad (5.30)$$

We then obtain with

$$V_{itmax}/V_o = 3.5,\ 2.0,\ \text{and}\ 1.5\ 10^{-3},$$

the values of

$$'t_a'$$

quoted in the table, with values also of t_f and t_{nom}

TABLE 3

	P	P/2	P/4	T/2	
$F_{1max.th.}$	11.4	4.35	1.90	0.693	10^{-2} eV/m
$F_{1max.exp}$	4.5	2.2	0.77	1.0	10^{-2} eV/m
t_{nom}	1.06	3.45	8.86	41.5	sec
t_f	1.19	3.94	10.1	46.5	sec
t_a	15.6	25.9	50.5	60.1	R^{-1}, at 3.5mrad
	3.54	5.82	11.3	13.7	R^{-1}, at 2.0mrad
	1.68	2.75	5.35	6.56	R^{-1}, at 1.5mrad
t(exp)	.65	2.5	7.5	5.5*	sec

* amplitude dependent(value at 2mrad)

As can be seen from the table, t_f is always substantially longer than t(exp), suggesting that an important adiabatic contribution is required. With R about 1 the t_a given contribute with something like the right order of magnitude in the right direction. But we have no particular reason for taking this rather than any other value of R, or indeed for supposing R to be constant from case to case or amplitude to amplitude. A serious estimate of t_a, and indeed of t_{nom}, requires a more detailed analysis of what is actually happening in the experiment than has been attempted.

A more detailed description of all aspects of this experiment will be found in [27].

ACKNOWLEDGEMENTS.

We would like to thank C.Rubbia and S.Van der Meer with whom we initiated this study, and also thank our colleagues S.Cittolin, L.Hoffmann, H.Koziol, G.Lebee, P.Lefevre, D.Mohl, H.Poth, B.Sadoulet, T.Sherwood, D.Simon, G.Stefanini, C.Taylor, L.Tecchio, L.Thorndahl, B.Vosicki, T.Wikberg for encouragement and contributions.We also acknowledge the untiring efforts of F.Cataneo, R.Charles, E.Chesi, R.Desperier, W.Glessing, M.Hauer, K.Muhleman, R.Pintus, and G.Pozzo during the preparation and the running of this experiment. We are indebted to J.S.Bell for assistance with typing the draft, and to him and A.Sørensen for aid with theory.

REFERENCES

1. G.I.Budker, Atomic Energy 22,No.5,346(1967).
2. G.I.Budker et al., Part.Acc.7,197(1976).
3. M.Bell et al., Phys.Lett.87B,275(1979)
4. Ya.S.Derbenev,A.N.Skrinsky,Part.Acc.8,1(1979).
5. Ya.S.Derbenev,A.N.Skrinsky,Part.Acc.8,235(1978).
6. Ya.S.Derbenev,I.Meshkov,CERN 77-08/PS.
7. F.Mills(FERMILAB),(Unpublished).
8. M.Rosenbluth,(Unpublished).

9. A.H.Sørensen,Preliminary internal reports,Institute of Physics,University of Aarhus,Denmark(1978).

1.Calculations on electron cooling.

2.Influence of a strong longitudinal magnetic field on electron cooling.

10. M.Bell,Part.Acc.10,101(1980).

11. J.R.Pierce,Bell System Technical Journal 30,825(1951).

12. W.Herrmannsfeldt,SLAC-166(1973).

13. M.Bell et al.,p-LEAR-Note 29(1979).(Talk by F.Krienen at Workshop on Physics with cooled low-energetic anti protons,Karlsruhe,1979).

14. T.R.Sherwood,CERN,Computer program developed from that of ref.12.

15. C.Rubbia,CERN EP-INT-NOTE 77-4,1977.

16. B.Schnizer,Diagnostics for transverse electron velocities in a beam in a magnetic field (1977).

Synchrotron radiation emitted by slow electrons within a straight circular waveguide.(Unpublished,Univ.of Graz).

B. Schnizer and E. Farnleitner,Acta Physica Austriaca 52,225-241 (1980).

17. C.Taylor and S.Hancock,CERN, unpublished.

18. M.Bell and J.S.Bell,TH-3054-CERN,March 1981.

19. S.Cittolin,B.Taylor.CAVIAR.Proceedings of the Joint Conference on 'Microprocessors in Automation and Communications',Univ. of Kent,Sep.1978.

20. B.Vosicki,K.Zankel,IEEE Transactions on Nuclear Science Vol.NS.22,no 3,1975,pp 1475-1478.

G.Stefanini,CERN, A profile monitor for low-intensity

circulating

beams, unpublished.

21. G. Carron et al. Experiments on stochastic cooling in ICE. IEEE Trans. on Nuclear Science,Vol.NS-26 No.3,June 1979.

22. E.N.Dementiev et al., CERN/PS/AA 79-41(Translation from preprint of the Institute for Nuclear Physics,(Novosibirsk,1979).

23. M.Bell,EP Internal Report 79-10(1979).

24. L.Spitzer Jr.,Physics of Fully Ionized Gases.(Wiley,New York, 1962).

25. F.Krienen,Proceedings of the 11th International Conference on High-Energy Accelerators.July 7-11,1980.

26. J.S.Bell and M.Bell,TH-3017-CERN,Jan.1981.

27. P.Møller-Petersen,Thesis to be submitted to Univ.of Aarhus, Denmark.

Figure Captions.

1.Photograph of electron cooling device.

2.Schematic assembly drawing of the cooling device.

3.The electron gun.

4.Calculated electron trajectories in gun.

5.Final transverse energy of the electrons at various radii in steps of 5mm, as a function of magnetic field. The calculation is for full perveance at 60kV anode voltage. The chosen working point is at the 700gauss minimum.

6.The collector.

7.Computed trajectories (solid lines) and electric field equipotentials (dotted lines)(including space charge effects)

at collector.

8.The ICE storage ring.

9.Measured frequency spectrum of the RF energy radiated by 25.9kV electrons in a magnetic field of 454.3 gauss. f_c = cyclotron frequency.

10.Schematic diagram of the high voltage system.

11.Collector perveance $P_{co}=I.V_{co}^{-3/2}$ as a function of beam current I.(P and P/2 operation).

12.Relative loss current as a function of electron gun high voltage for P and P/2 operation.

13.Cross-sections of neutral atom beam as seen by the two-dimensional MWPC. The principal axes of the ellipses show, on a 2.5 times enlarged scale, the r.m.s. widths of the horizontal and vertical profiles respectively.

(a) Frame number

(b) Acquisition time

(c) Number of wires hit

(d) Horizontal position (average) mm

(e) Vertical position (average) mm

(f) Horizontal width rms mm

(g) Vertical width rms mm

14.Profiles observed by the horizontal BPM with 1mm and .3mm slit widths in the drum of the mechanical scanning system.

15a.Frequency spectrum of Schottky noise, taken at the beginning and end of the cooling process,at the 24^{th} harmonic of the revolution frequency.

15b.Similar spectrum of a low intensity cooled beam. $I=8.10^6$ protons. $\delta p/p(FWHM) \simeq 4.10^{-5}$.

16. Equilibrium momentum spread of 45MeV protons versus intensity.

(o) temperature limited T/2 electron beam (590mA).

(▽) space charge limited P/2 electron beam (1250mA).

17. Betatron oscillation cooling following a coherent kick.

18. Total damping times as a function of amplitude for various gun modes.

a Full P gun

b P/2 gun

c P/4 gun

d T/2 gun

19. Damping rates,(a), and cooled proton relative momentum spread,(b), as a function of longitudinal electron velocity spread.

20. Measured values of F_1

(o) P/2 gun.

(▽) P/2 gun but with an extra 1kHz sine wave.

. T/2 gun.

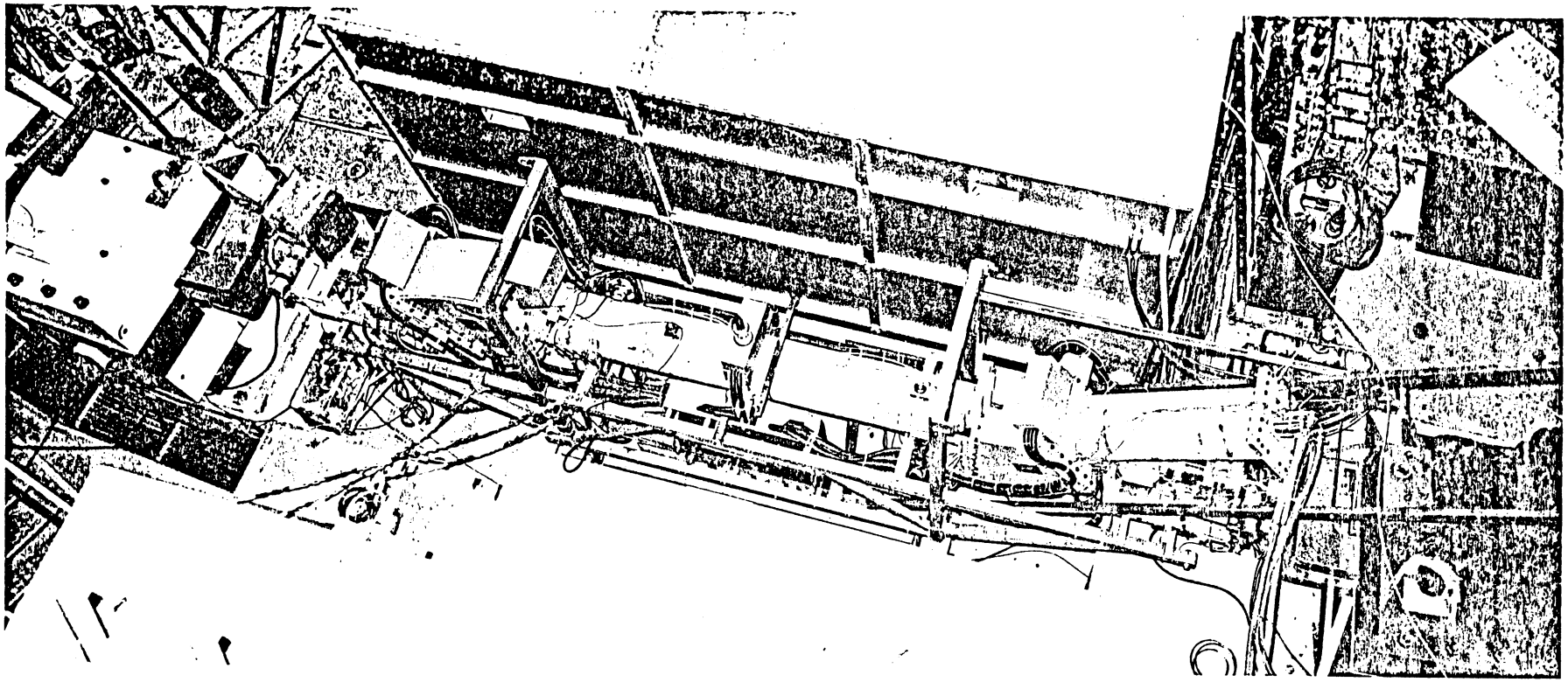

Fig.1

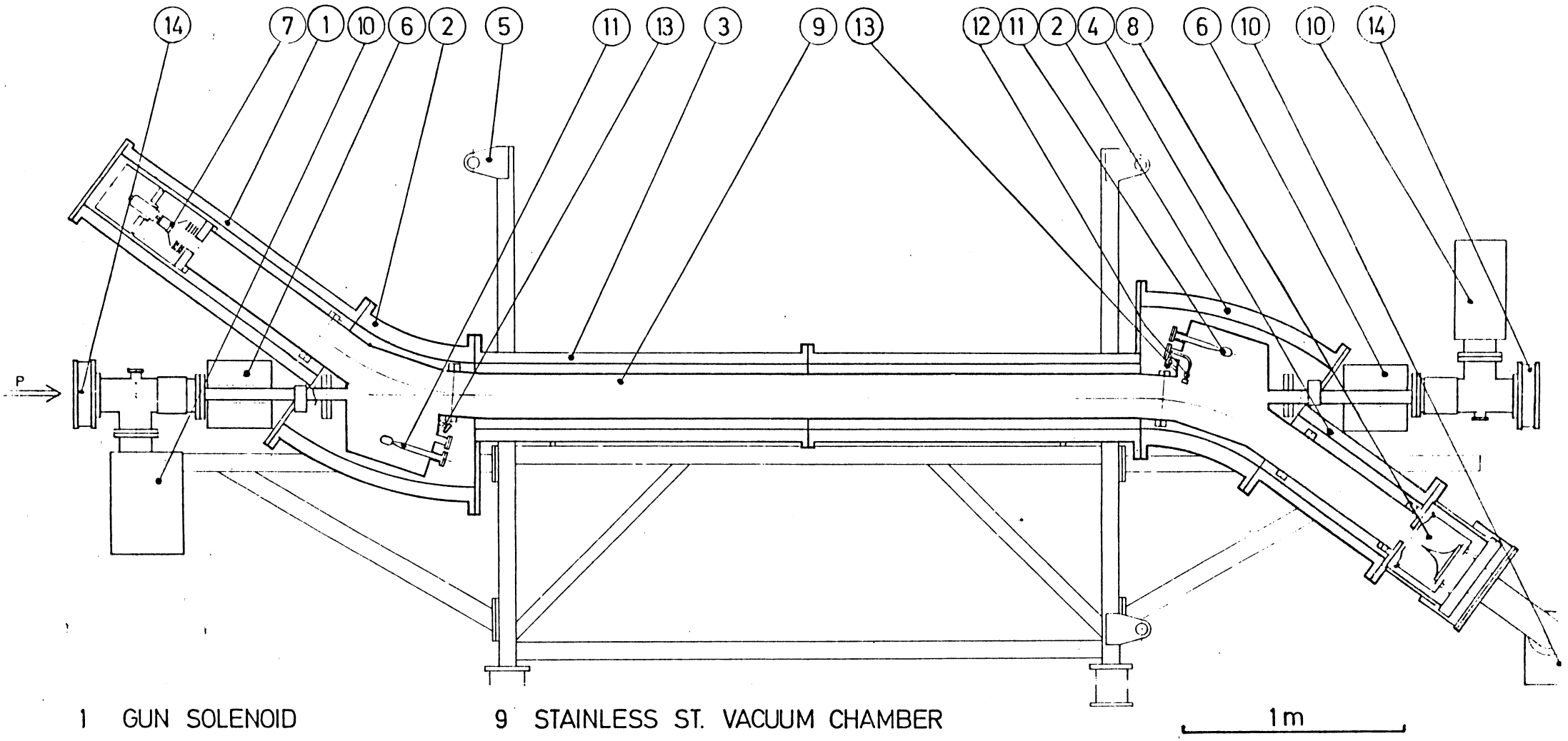

1 GUN SOLENOID
2 TOROID
3 CENTRAL SOLENOIDS
4 COLLECTOR SOLENOID
5 SUPPORTING FRAME
6 CORRECTION MAGNET
7 ELECTRON GUN CATHODE
8 COLLECTOR
9 STAINLESS ST. VACUUM CHAMBER
10 VACUUM PUMP (SPUTTER-ION)
11 VACUUM PUMP (Ti-SUBLIMATION)
12 SYNCHROTRON RADIATION ANTENNA
13 VIEWING PORT
14 SECTOR VALVE

Fig.2

1	CATHODE	W
2	PIERCE SHIELD	Ta
3	HEAT SINK	Mo
4	GAS COOLED BASE	Cu
5	CATHODE FEEDTHROUGH	Al_2O_3
6	ANODE FEEDTHROUGH	Al_2O_3
7	BELLOWS	s. st.
8	ANODES	Ti
9	ANODE	Cu
10	ANODE SUPPORT	Al_2O_3

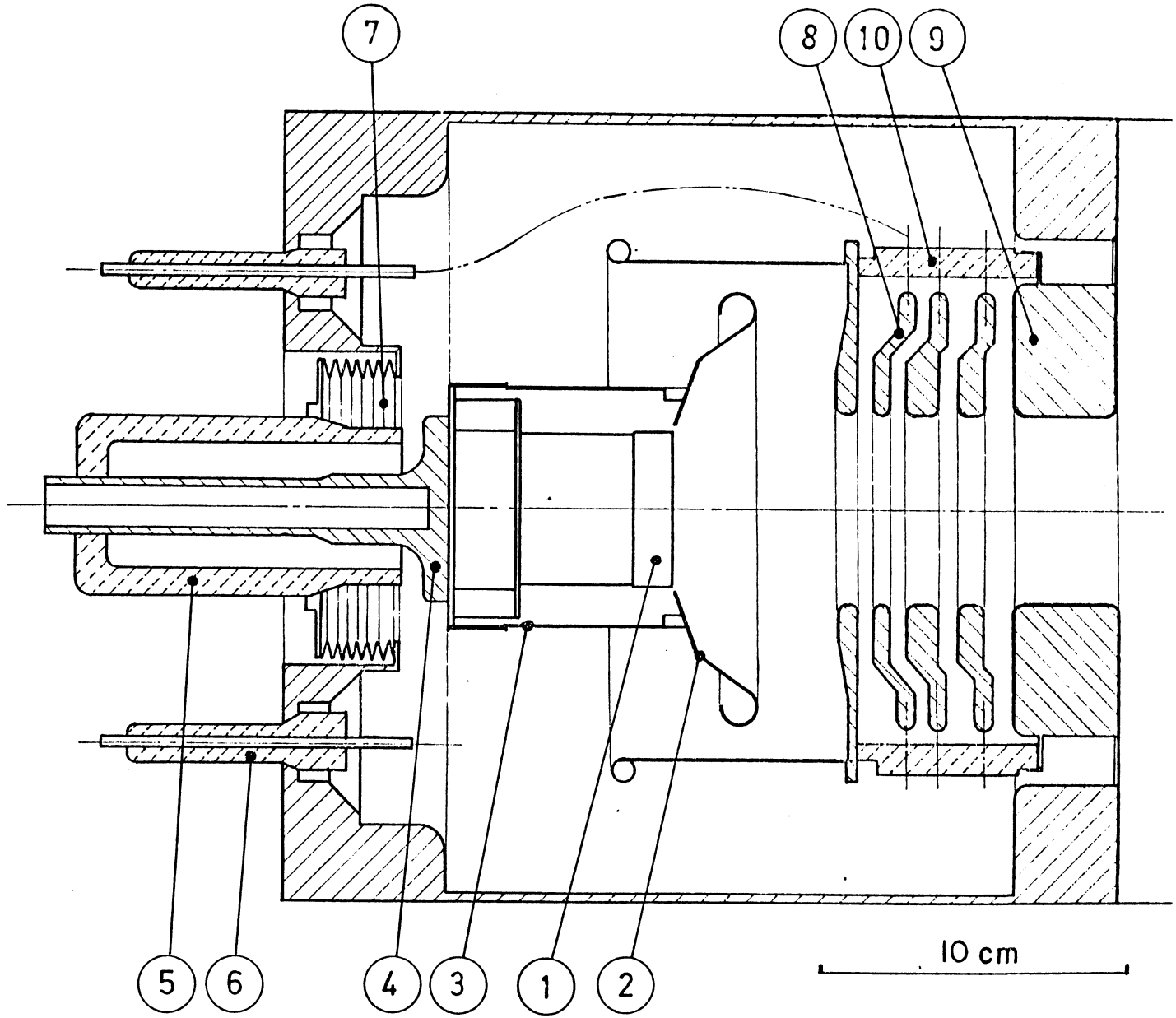

Fig.3

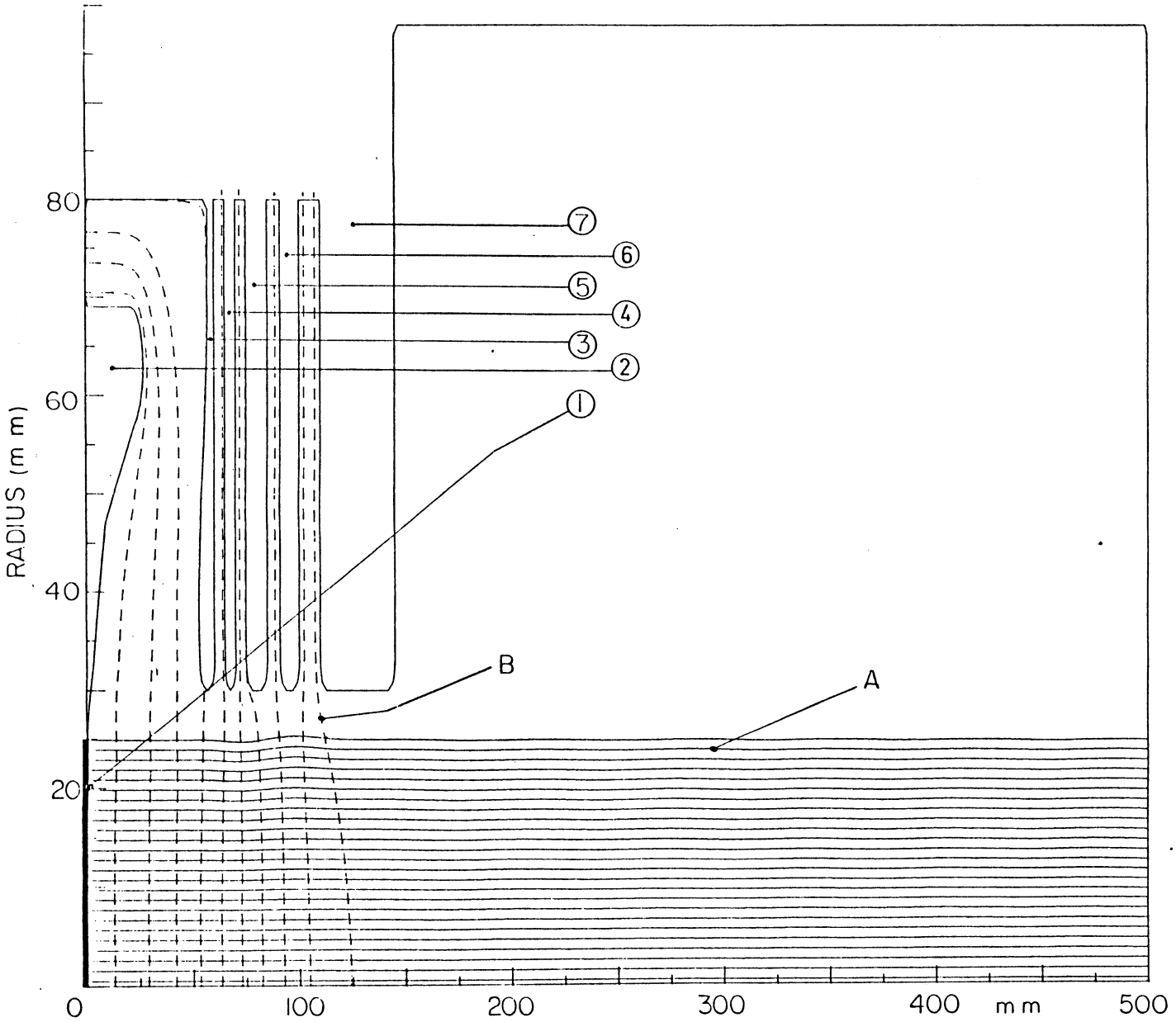

1 CATHODE
2 PIERCE SHIELD
3 1st. ANODE
4 2nd. ANODE
5 3rd. ANODE
6 4th. ANODE
7 5th. ANODE (PART OF DRIFT TUBE

A ELECTRON TRAJECTORY
B EQUIPOTENTIAL SURFACE (INCL. SPACE CHARGE EFFECTS)

Fig.4

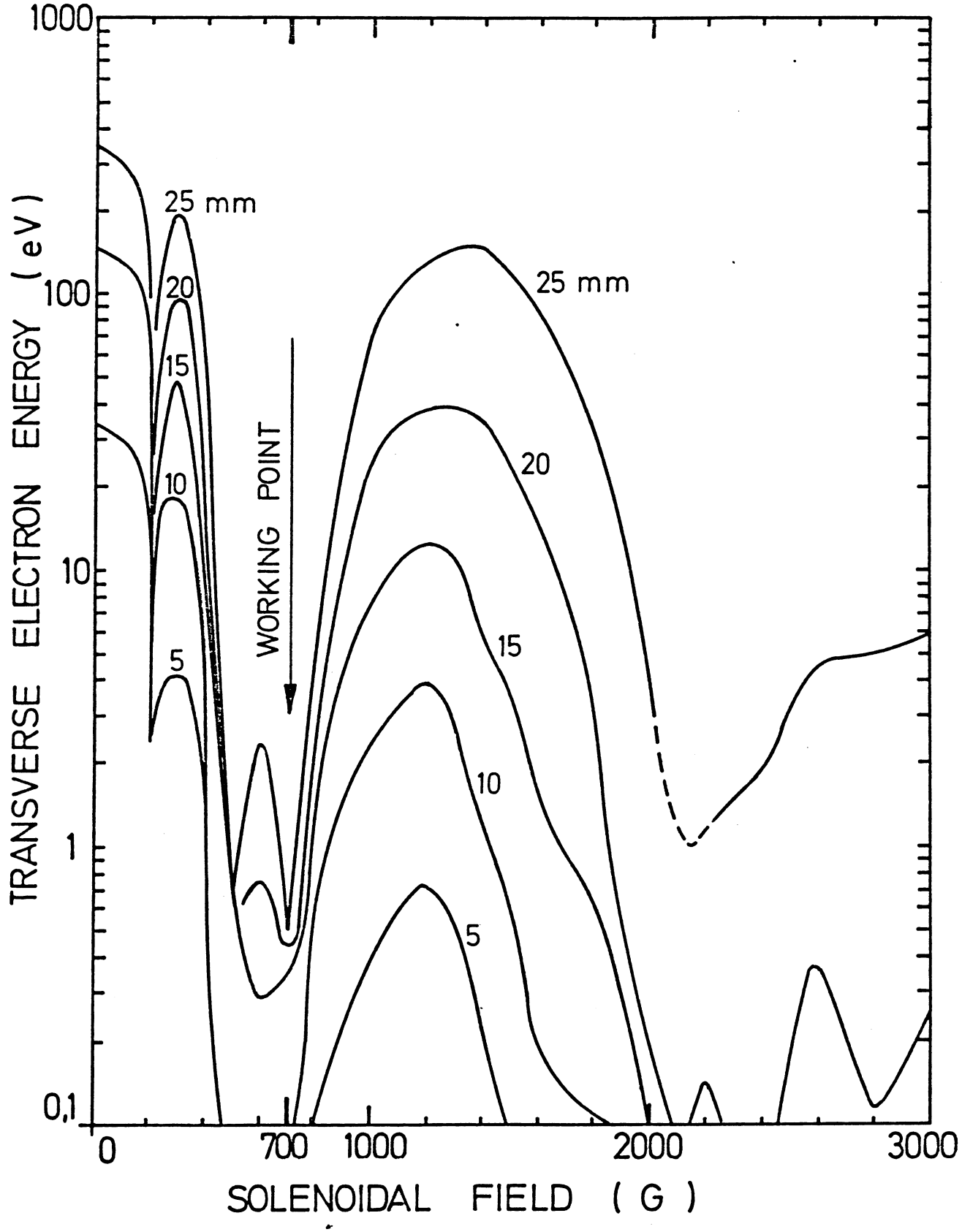
1000
100
10
1
0,1
TRANSVERSE ELECTRON ENERGY (eV)
25 mm
20
15
10
5
WORKING POINT
25 mm
20
15
10
5
0
700
1000
2000
3000
SOLENOIDAL FIELD (G)

Fig.5

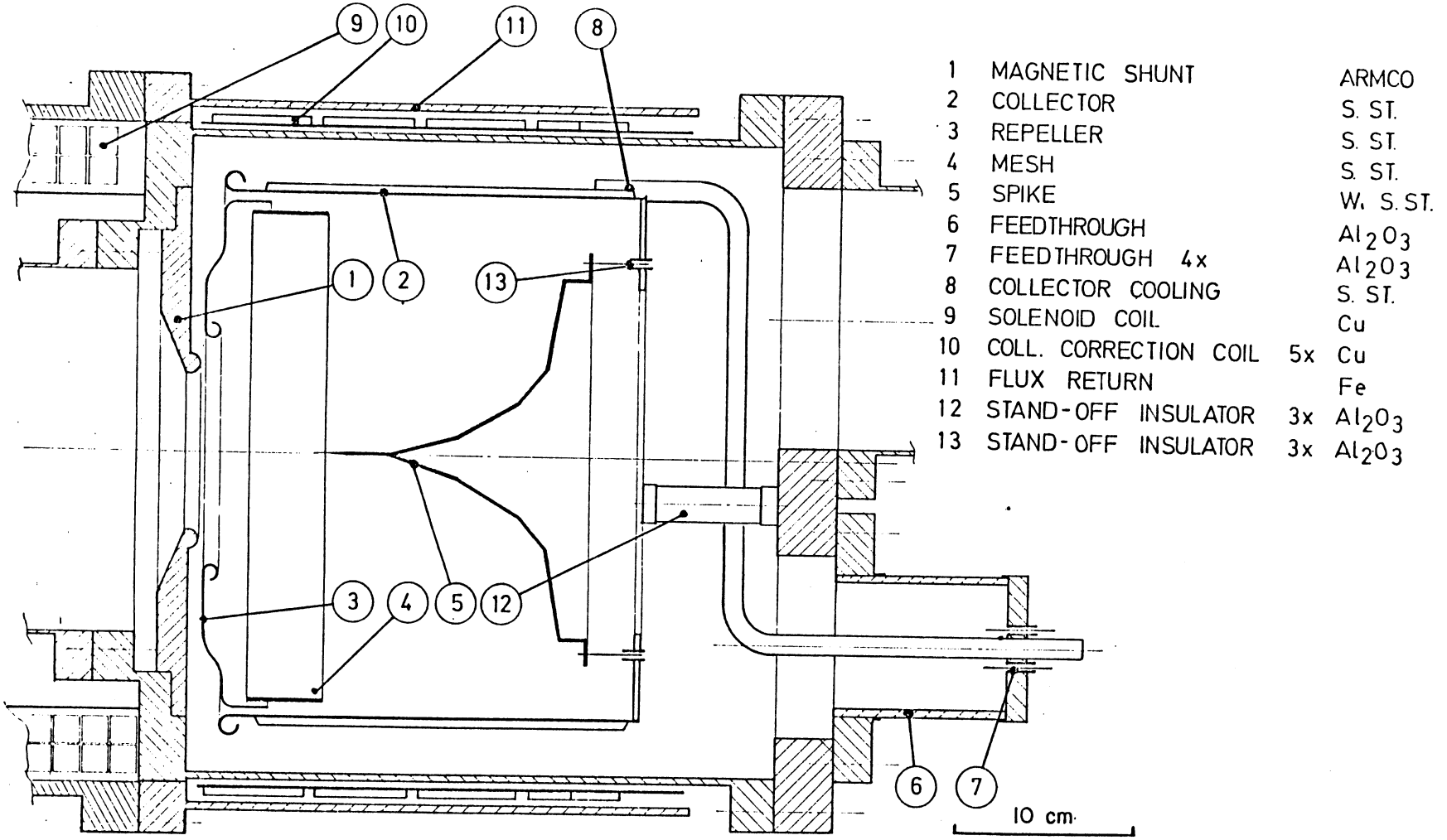

1	MAGNETIC SHUNT		ARMCO
2	COLLECTOR		S. ST.
3	REPELLER		S. ST.
4	MESH		S. ST.
5	SPIKE		W. S. ST.
6	FEEDTHROUGH		Al_2O_3
7	FEEDTHROUGH	4x	Al_2O_3
8	COLLECTOR COOLING		S. ST.
9	SOLENOID COIL		Cu
10	COLL. CORRECTION COIL	5x	Cu
11	FLUX RETURN		Fe
12	STAND-OFF INSULATOR	3x	Al_2O_3
13	STAND-OFF INSULATOR	3x	Al_2O_3

Fig. 6

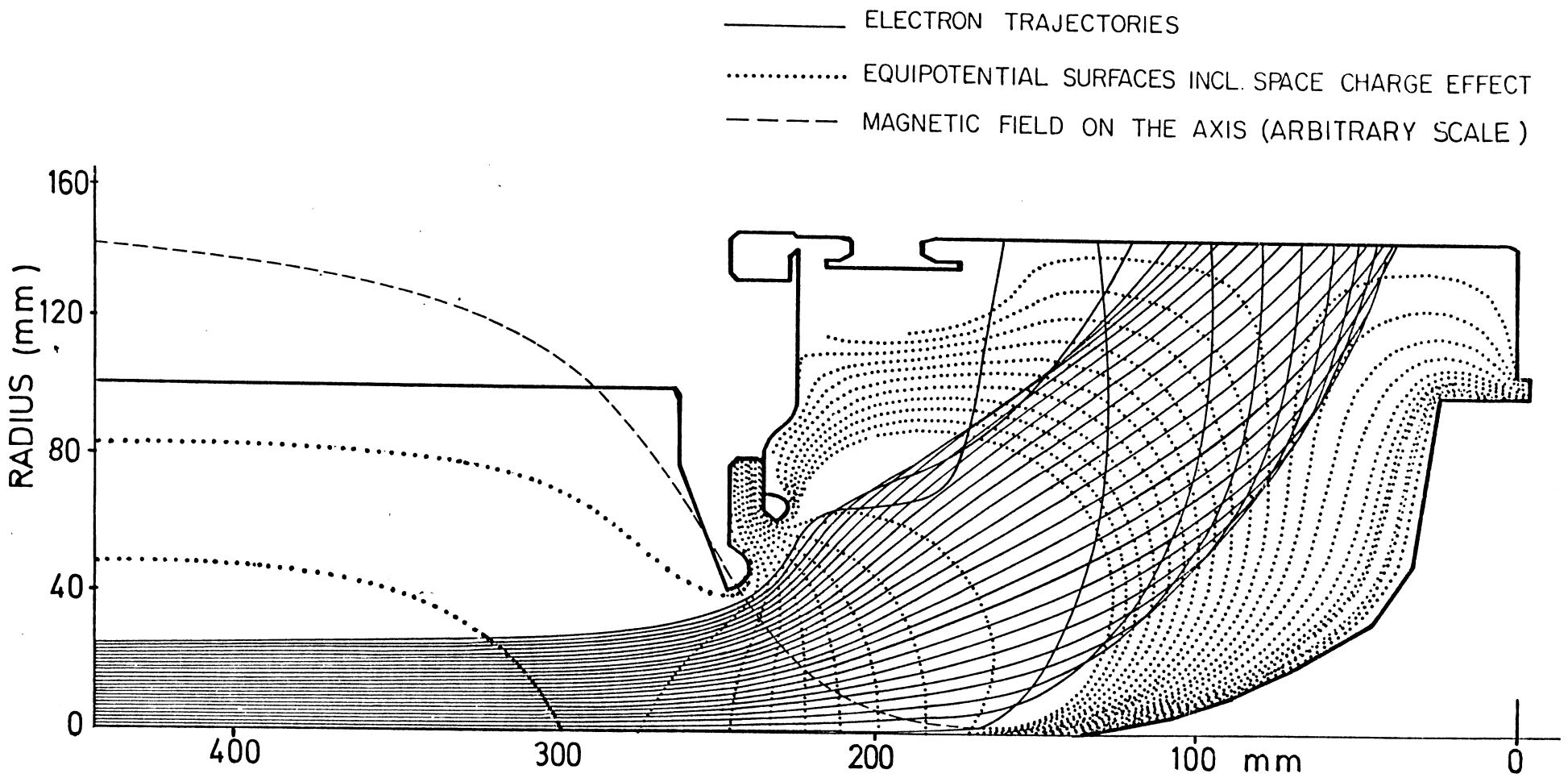
ELECTRON TRAJECTORIES
EQUIPOTENTIAL SURFACES INCL. SPACE CHARGE EFFECT
MAGNETIC FIELD ON THE AXIS (ARBITRARY SCALE)
RADIUS (mm)
160
120
80
40
0
400
300
200
100 mm
0

Fig.7

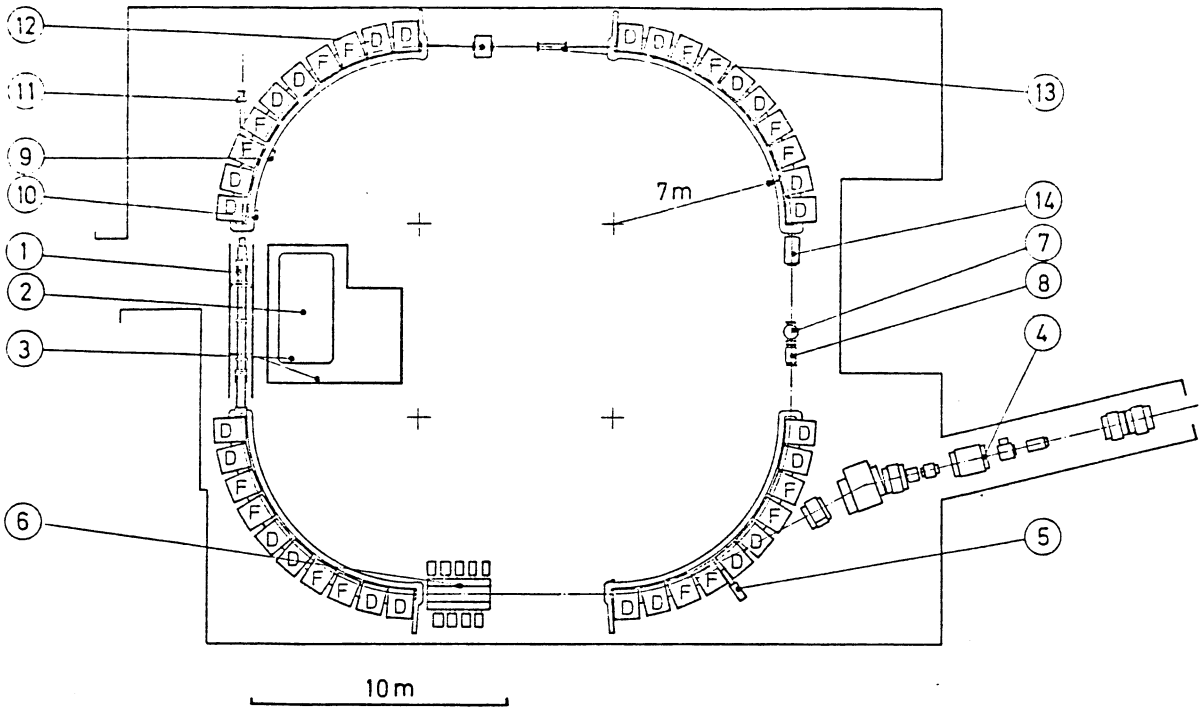

1 ELECTRON COOLING DEVICE
2 HIGH VOLTAGE SUPPLY
3 FARADAY CAGE
4 TRANSFER LINE
5 INFLECTOR
6 FULL APERTURE KICKER
7 BEAM PROFILE MONITOR (HORIZ.)
8 BEAM PROFILE MONITOR (VERT.)
9 SCRAPER (HORIZ.)
10 SCRAPER (VERT.)
11 WIRE CHAMBERS
12 R.F. CAVITY
13 WIDE BAND KICKER (LONG.)
14 SCHOTTKY NOISE PICK-UP (LONG.)

Fig.8

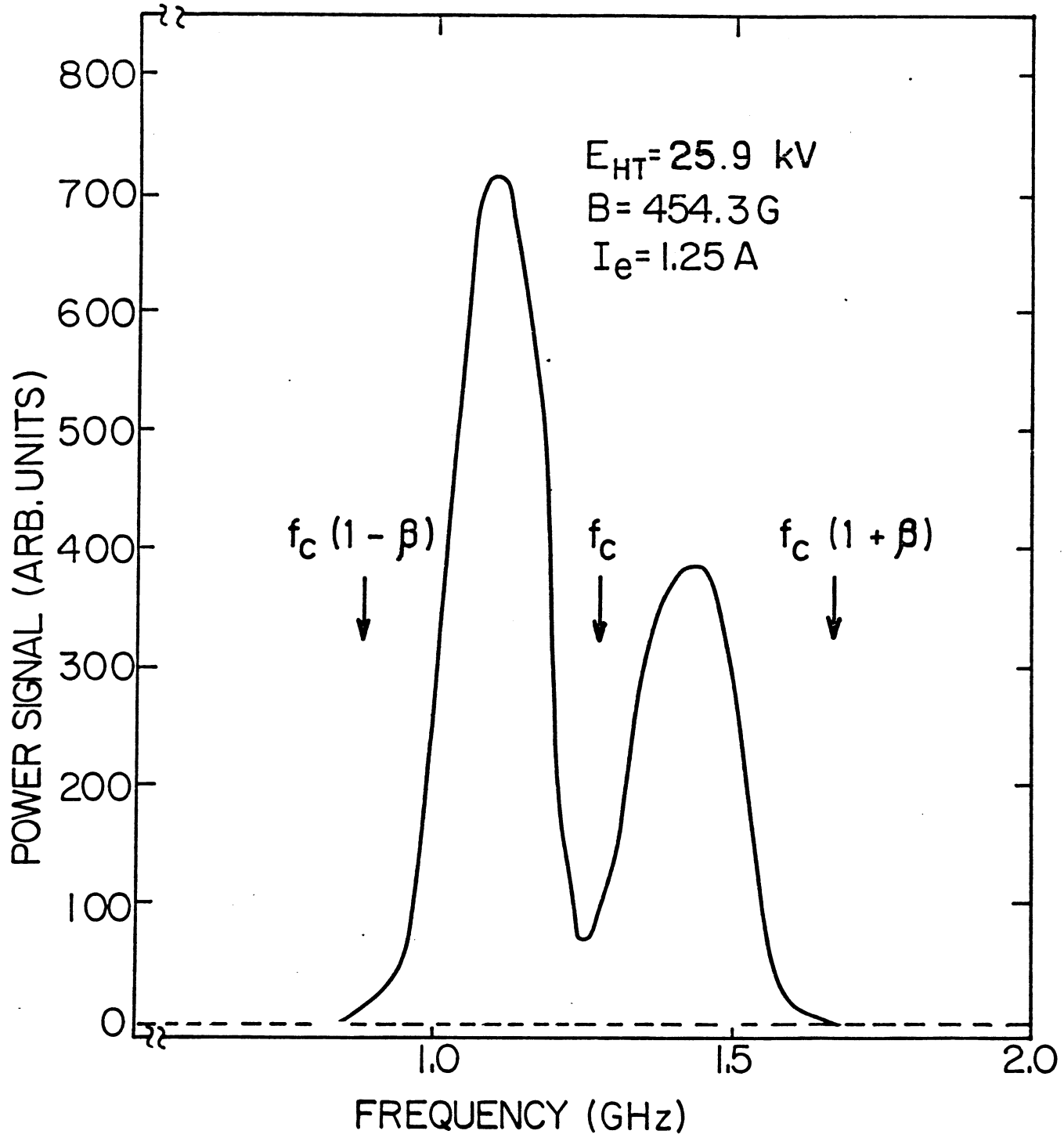
800
700
600
500
400
300
200
100
0
POWER SIGNAL (ARB. UNITS)
E_{HT}= 25.9 kV
B= 454.3 G
I_e= 1.25 A
f_c (1 - β)
f_c
f_c (1 + β)
1.0
1.5
2.0
FREQUENCY (GHz)

Fig.9

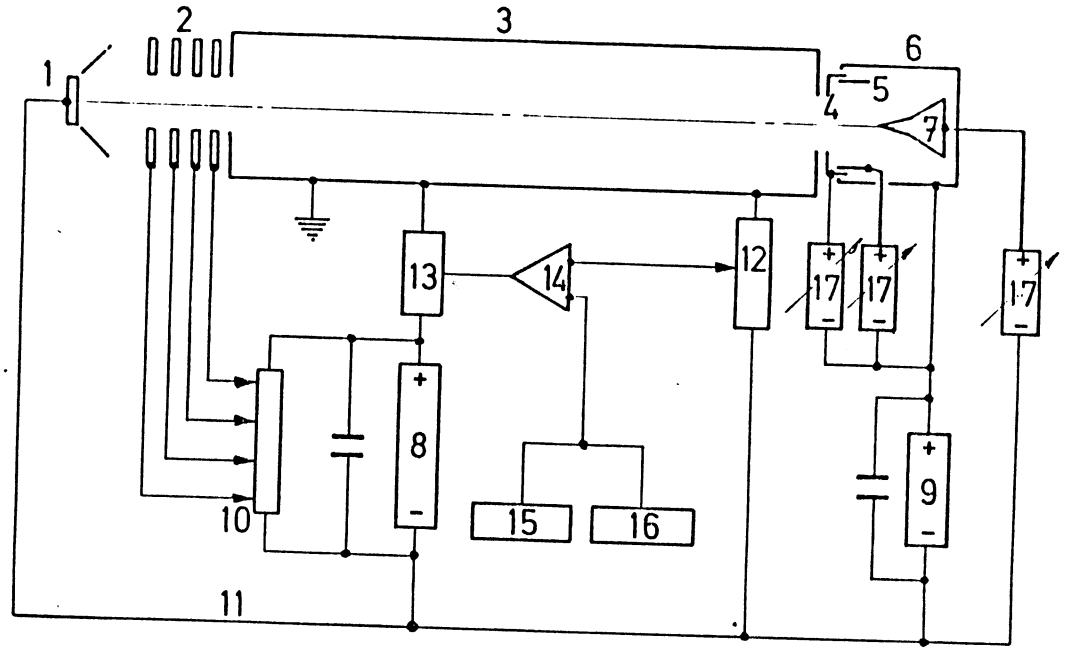

1 CATHODE
2 ANODES
3 DRIFT TUBE
4 REPELLER
5 MESH
6 COLLECTOR
7 SPIKE
8 ANODE POWER SUPPLY
9 COLLECTOR POWER SUPPLY
10 ANODE POTENTIAL DIVIDER
11 H.V. FARADAY CAGE COMMON
12 H.V. DIVIDER
13 STABILIZER
14 COMPARATOR
15 MODULATOR
16 REFERENCE
17 COLL. ELECTRODE SUPPLIES

Fig.10

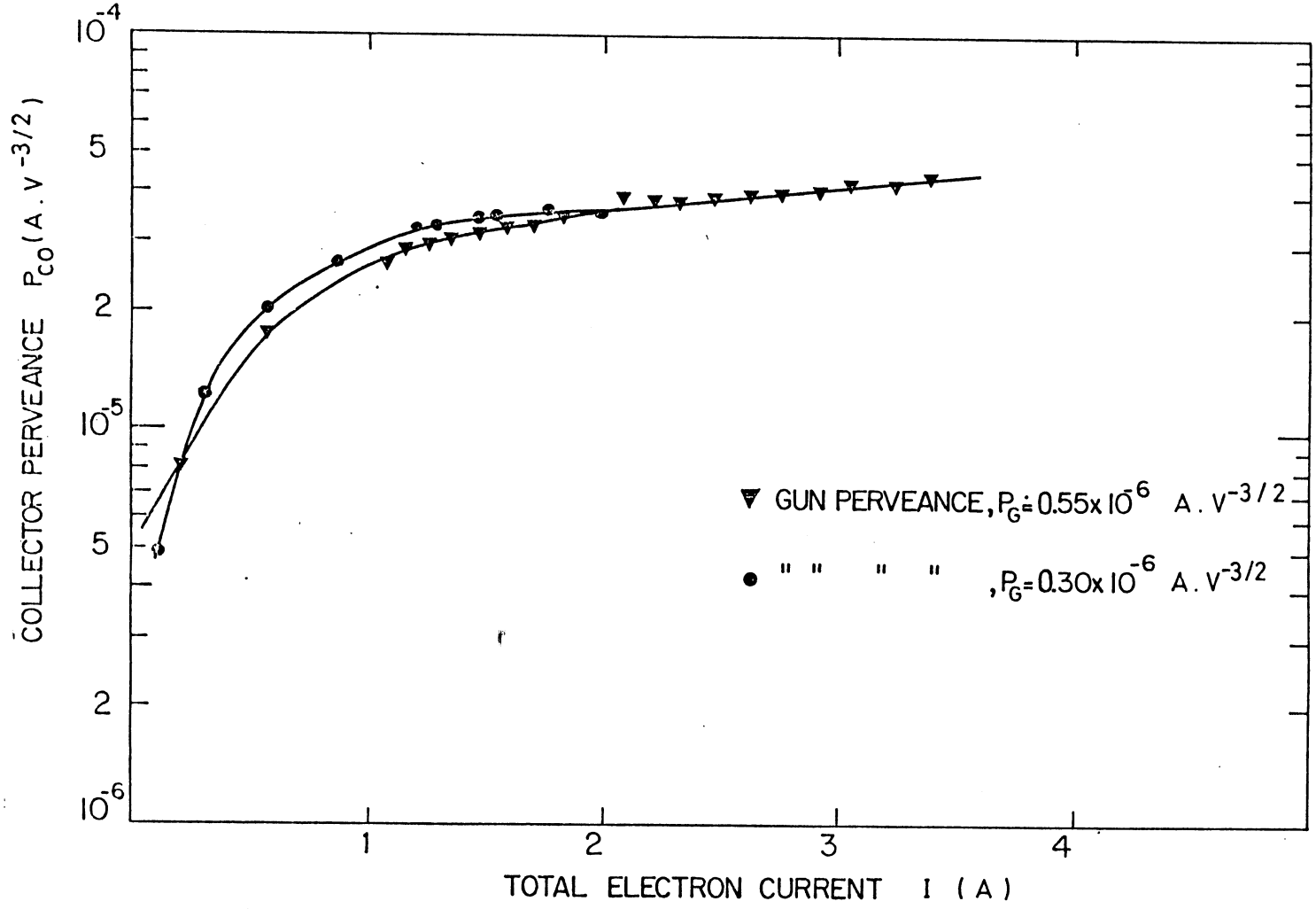
COLLECTOR PERVEANCE P_{CO} (A . V$^{-3/2}$)
10^{-4}
5
2
10^{-5}
5
2
10^{-6}
1
2
3
4
TOTAL ELECTRON CURRENT I (A)
GUN PERVEANCE, P_G = 0.55x 10^{-6} A . V$^{-3/2}$
" " " " , P_G = 0.30x 10^{-6} A . V$^{-3/2}$

Fig.11

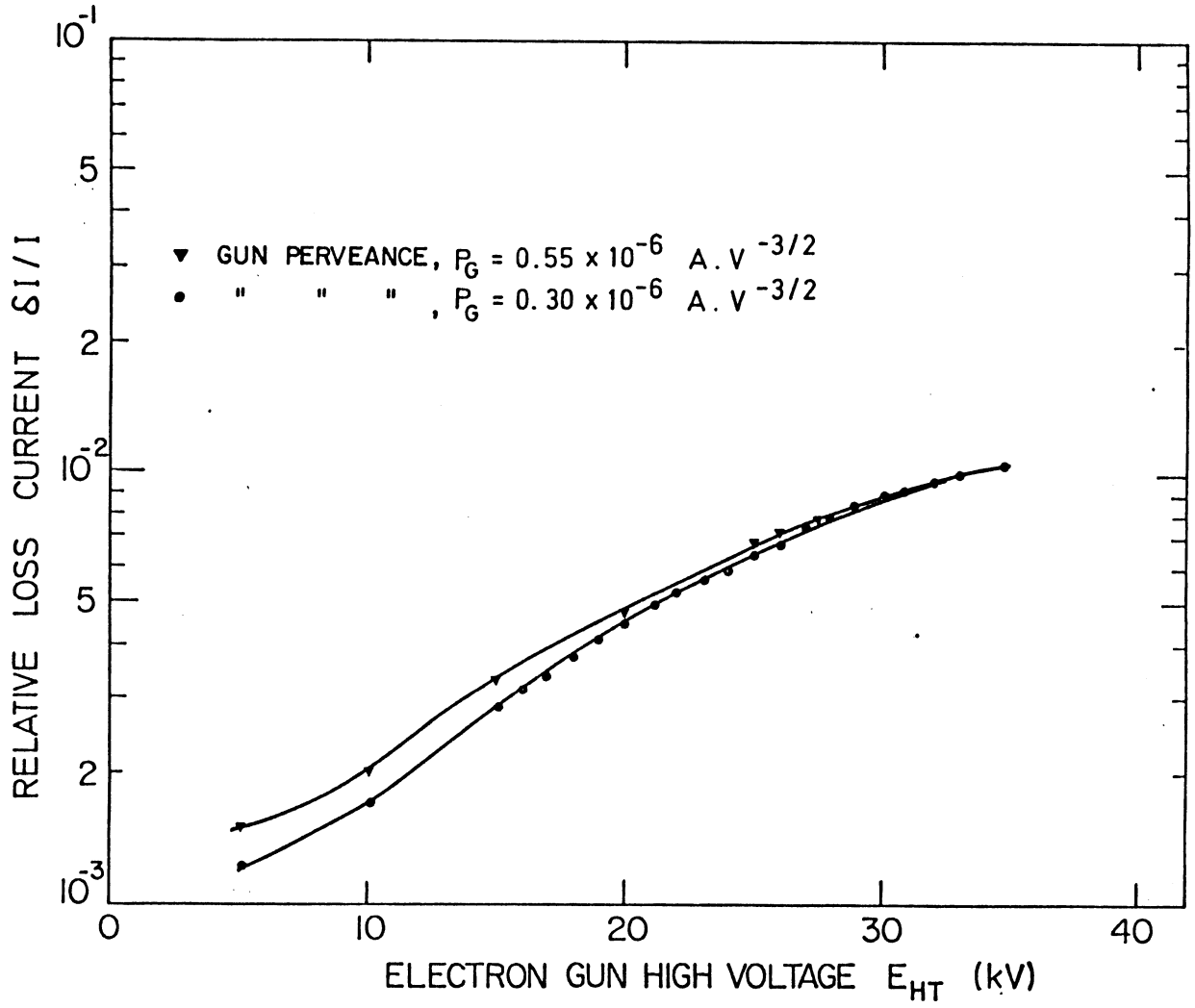
RELATIVE LOSS CURRENT δI/I
10^-1
5
2
10^-2
5
2
10^-3
0
10
20
30
40
ELECTRON GUN HIGH VOLTAGE E_HT (kV)
▼ GUN PERVEANCE, P_G = 0.55 x 10^-6 A.V^-3/2
● " " " , P_G = 0.30 x 10^-6 A.V^-3/2

Fig.12

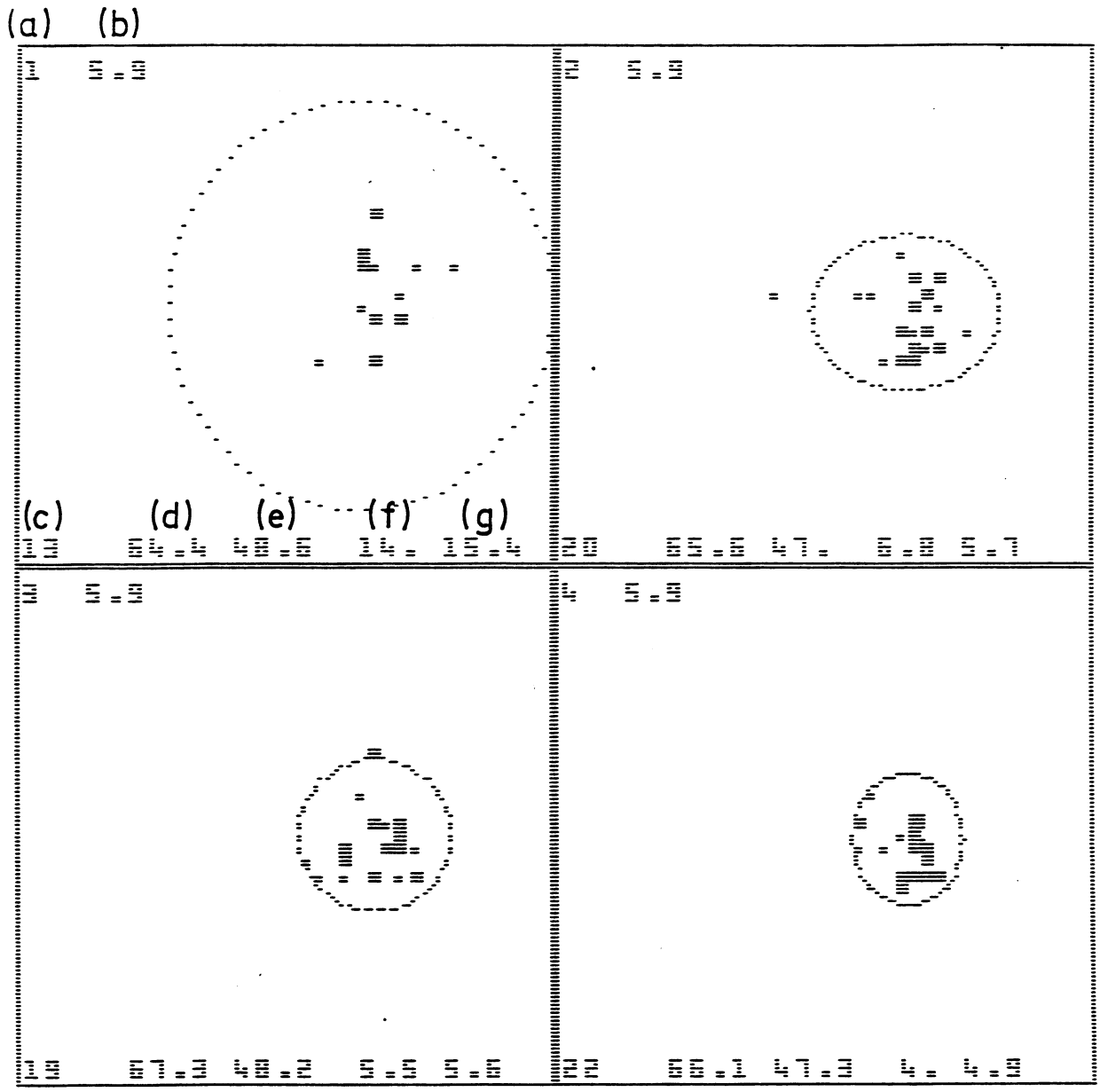

Fig.13

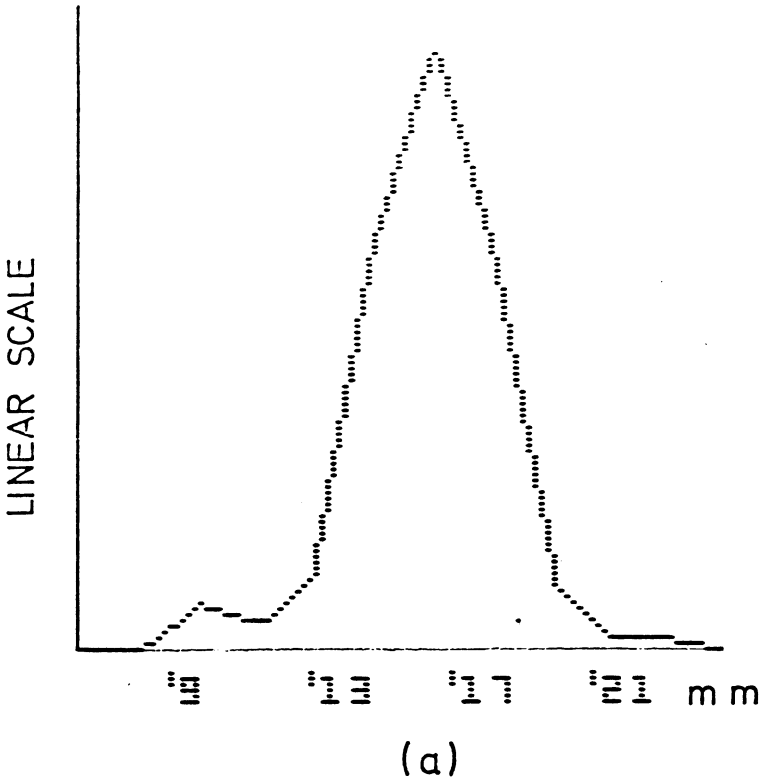

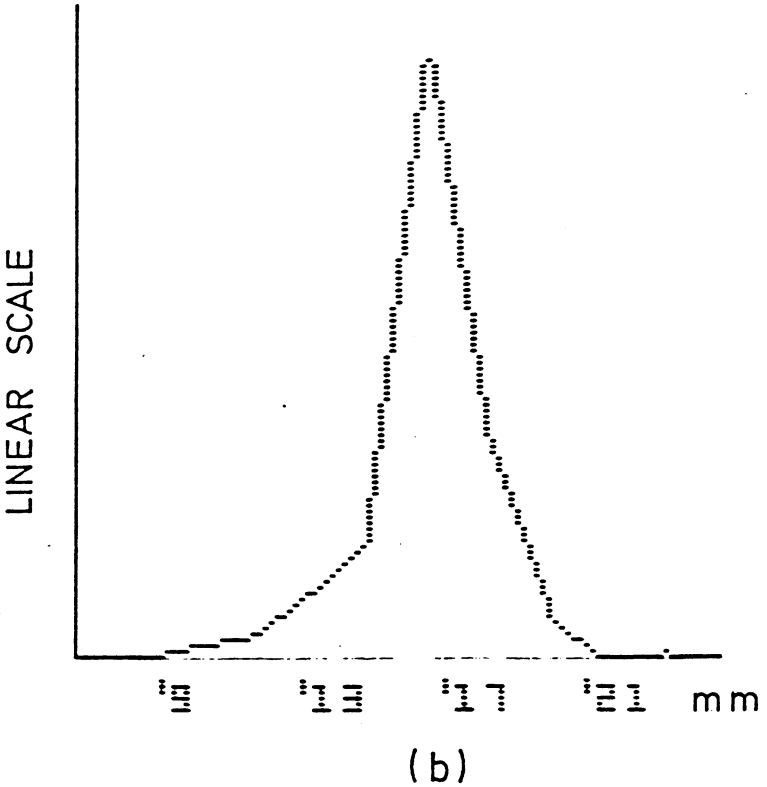

Fig.14

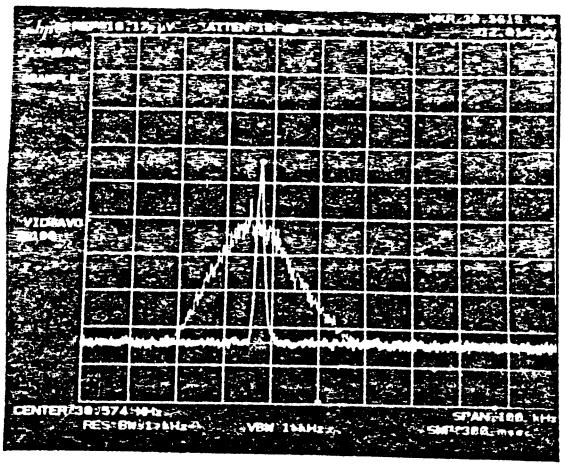

(a)

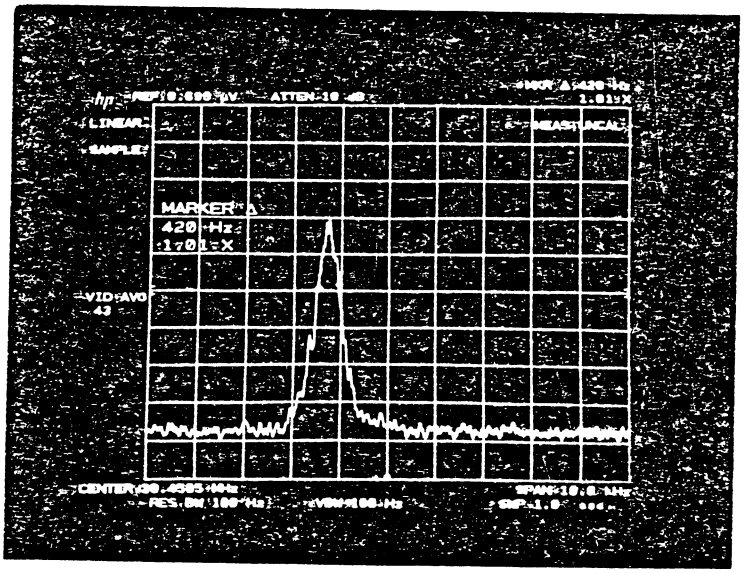

(b)

Fig.15

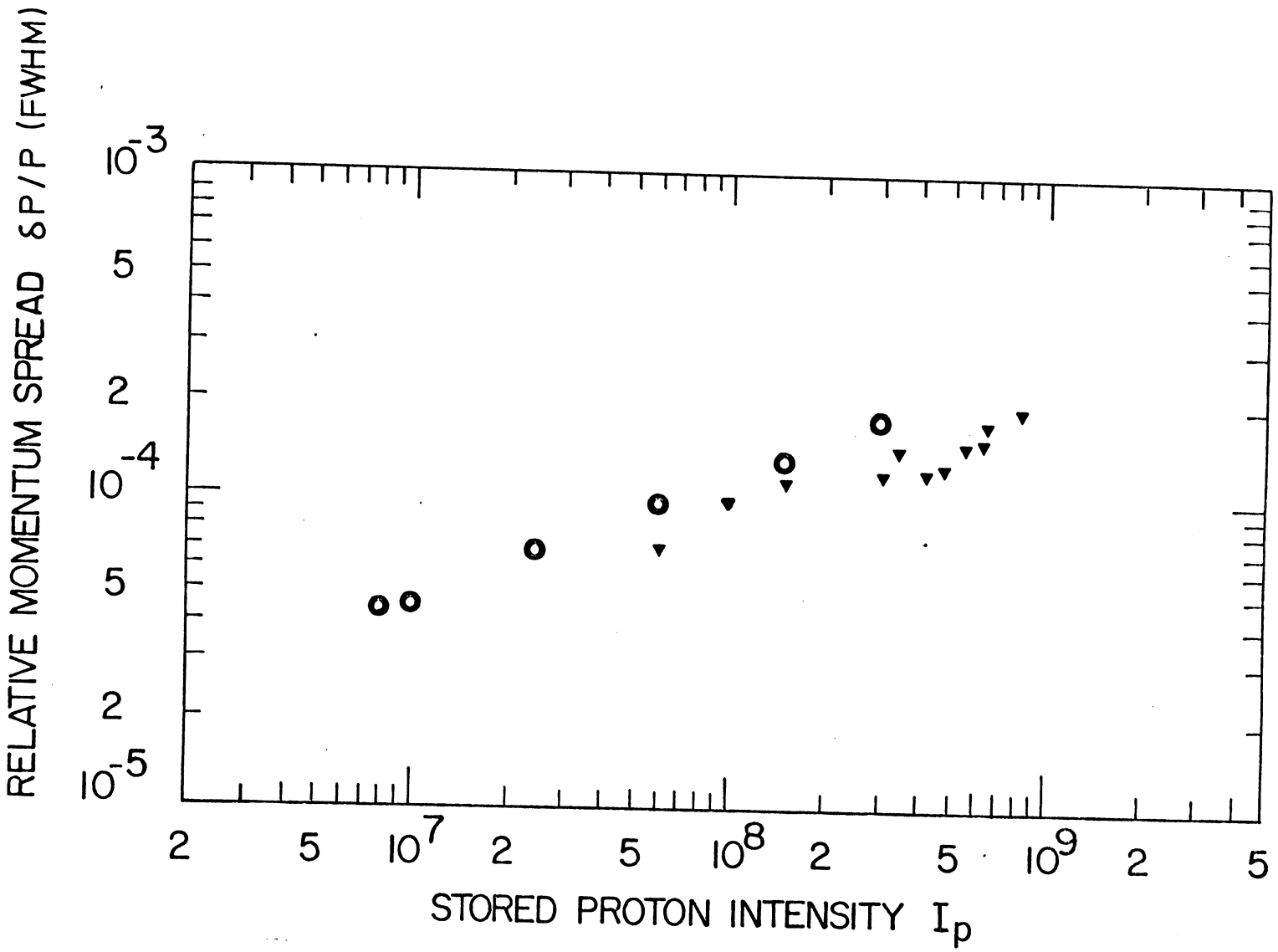
RELATIVE MOMENTUM SPREAD δP/P (FWHM)
10-3
5
2
10-4
5
2
10-5
2
5
10^7
2
5
10^8
2
5
10^9
2
5
STORED PROTON INTENSITY Ip

Fig.16

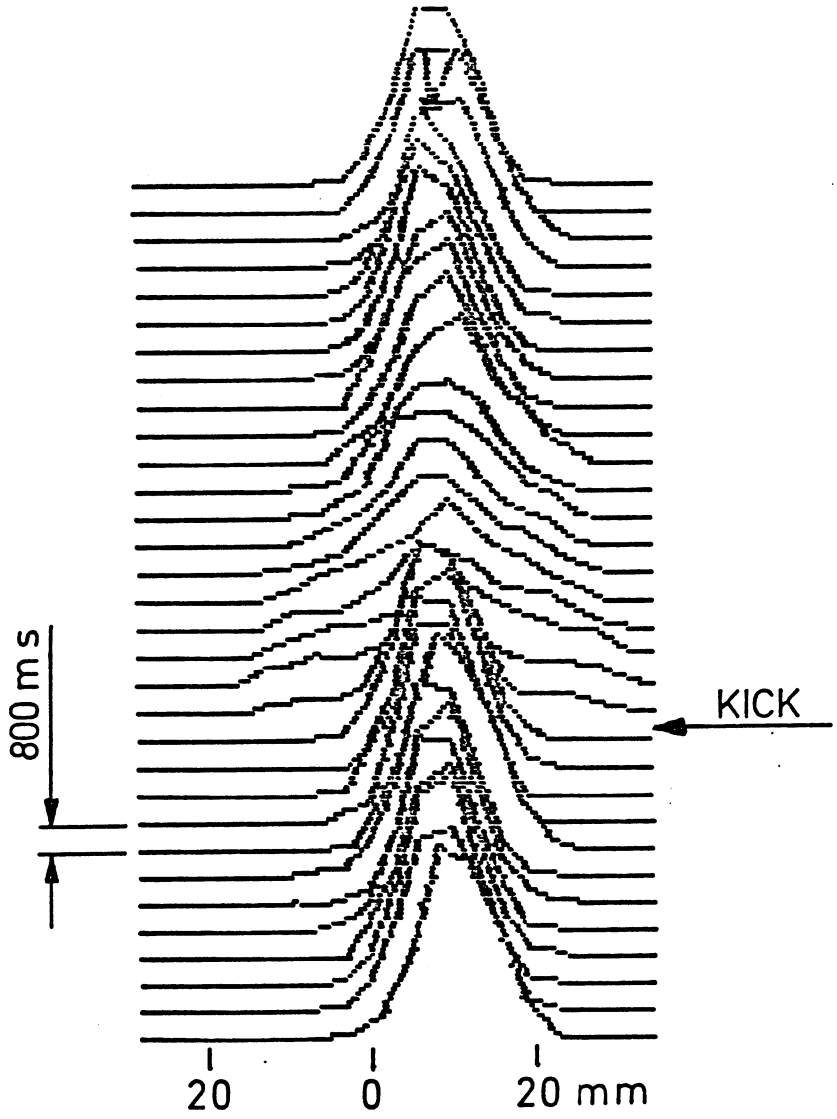

Fig.17

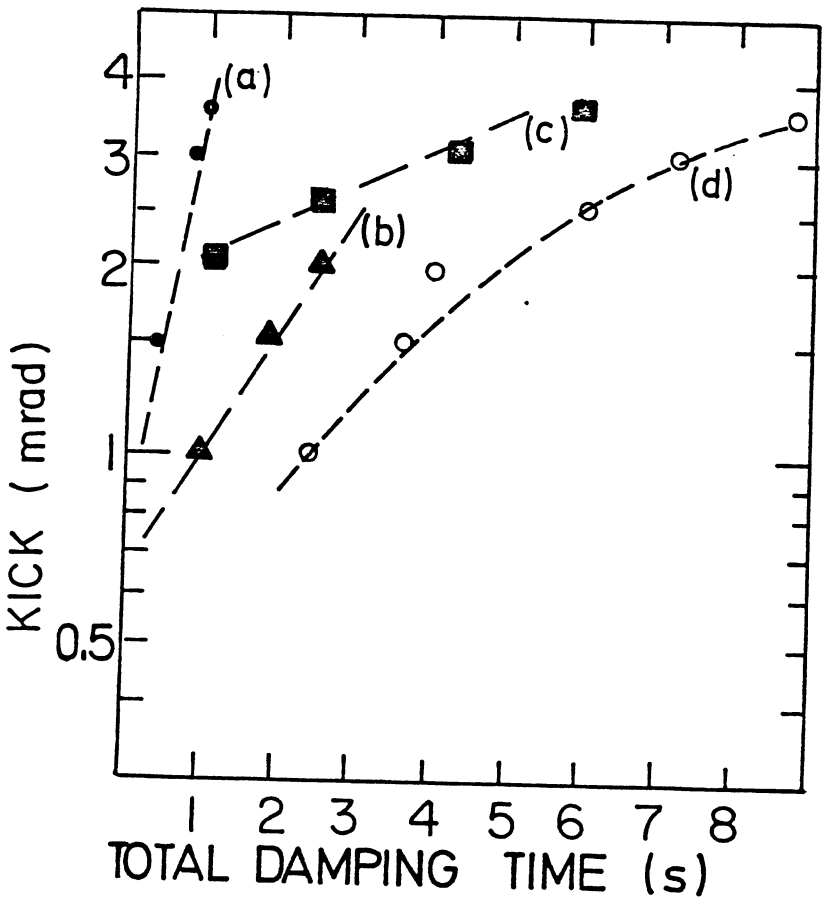

Fig.18

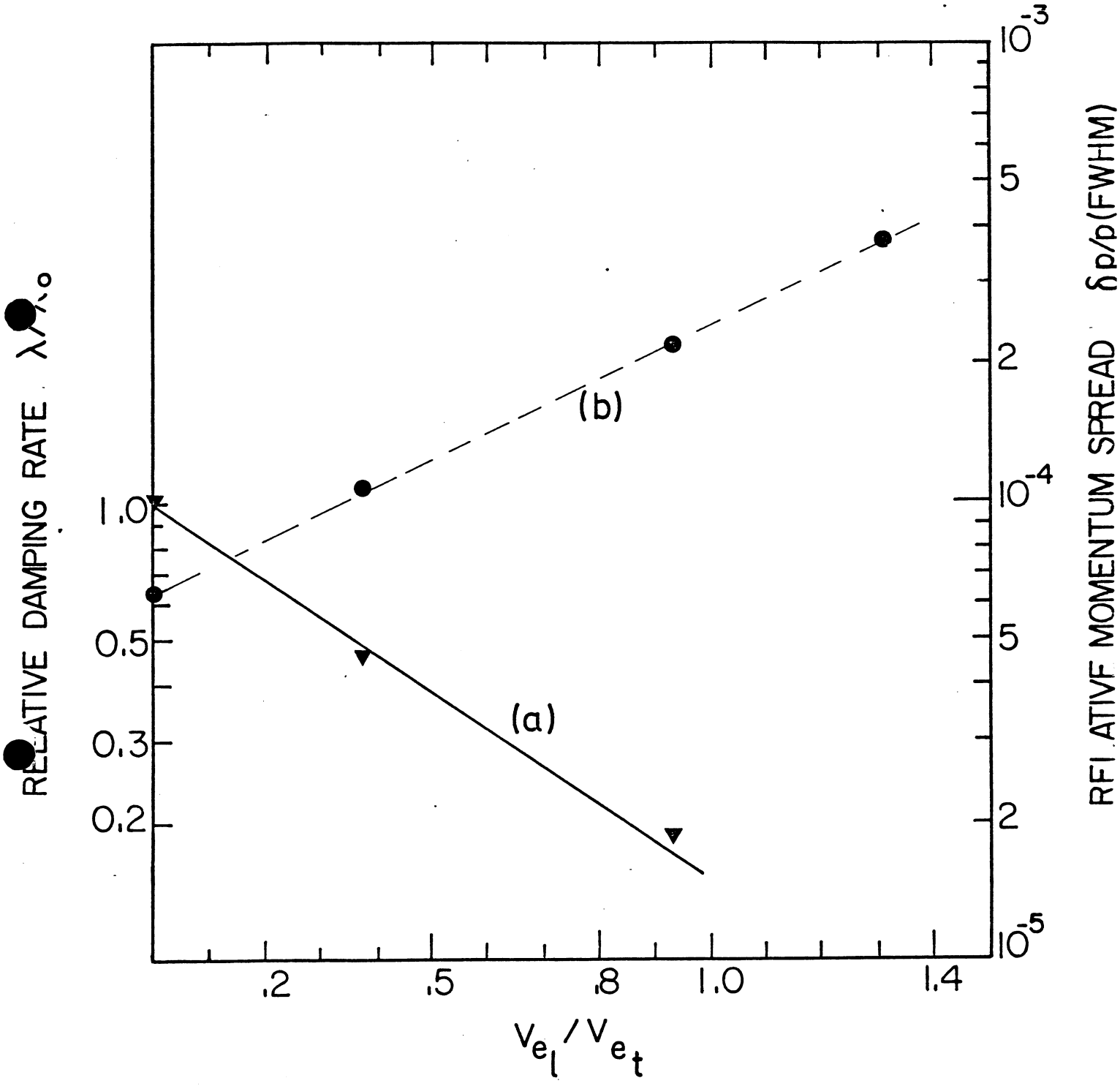
RELATIVE DAMPING RATE λ/λ₀
RELATIVE MOMENTUM SPREAD δp/p(FWHM)
1.0
0.5
0.3
0.2
10⁻³
5
2
10⁻⁴
5
2
10⁻⁵
(a)
(b)
.2
.5
.8
1.0
1.4
Vₑ∥ / Vₑ⊥

Fig.19

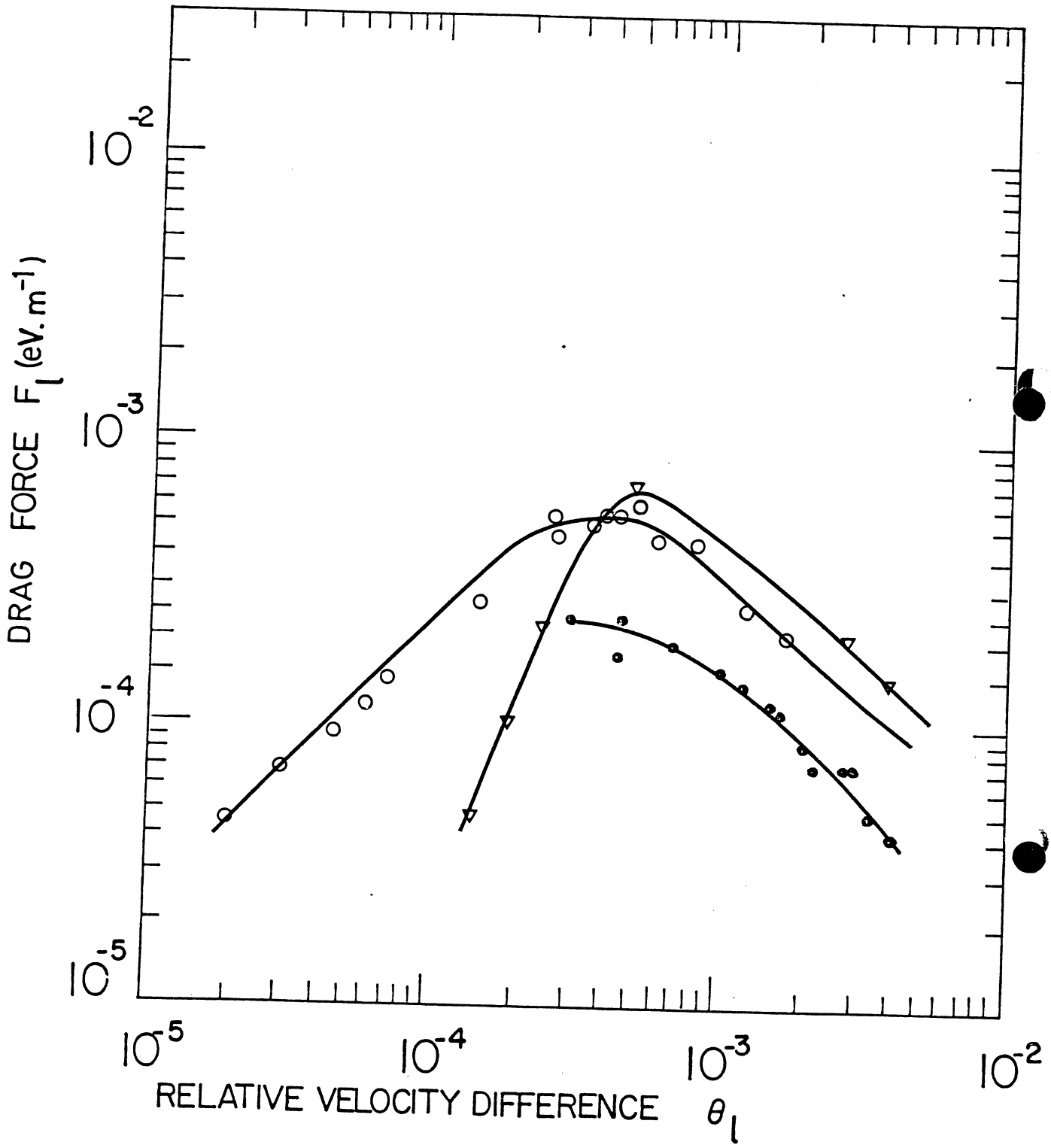
DRAG FORCE F_l (eV.m^{-1})
10^{-2}
10^{-3}
10^{-4}
10^{-5}
10^{-5}
10^{-4}
10^{-3}
10^{-2}
RELATIVE VELOCITY DIFFERENCE θ_l

Fig.20